ORIGINAL ARTICLE

An *Ixodes persulcatus* Inhibitor of Plasmin and Thrombin Hinders Keratinocyte Migration, Blood Coagulation, and Endothelial Permeability

JID Open

Markus Berger[1,2,8], Sheila Rosa da Mata[3,8], Nicolle Masseroni Pizzolatti[3], Luís Fernando Parizi[4], Satoru Konnai[5], Itabajara da Silva Vaz Jr.[4,6,7], Adriana Seixas[3,7] and Lucas Tirloni[1]

The skin is the first host tissue that the tick mouthparts, tick saliva, and a tick-borne pathogen contact during feeding. Tick salivary glands have evolved a complex and sophisticated pharmacological arsenal, consisting of bioactive molecules, to assist blood feeding and pathogen transmission. In this work, persulcatin, a multifunctional molecule that targets keratinocyte function and hemostasis, was identified from *Ixodes persulcatus* female ticks. The recombinant persulcatin was expressed and purified and is a 25-kDa acidic protein with 2 Kunitz-type domains. Persulcatin is a classical tight-binding competitive inhibitor of proteases, targeting plasmin (K_i: 28 nM) and thrombin (K_i: 115 nM). It blocks plasmin generation on keratinocytes and inhibits their migration and matrix protein degradation; downregulates matrix metalloproteinase 2 and matrix metalloproteinase 9; and causes a delay in blood coagulation, endothelial cell activation, and thrombin-induced fibrinocoagulation. It interacts with exosite I of thrombin and reduces thrombin-induced endothelial cell permeability by inhibiting vascular endothelial-cadherin disruption. The multifaceted roles of persulcatin as an inhibitor and modulator within the plasminogen−plasmin system and thrombin not only unveil further insights into the intricate mechanisms governing wound healing but also provide a fresh perspective on the intricate interactions between ticks and their host organisms.

Keywords: Coagulation, Protease inhibitors, Ticks, Tick saliva, Wound healing

Journal of Investigative Dermatology (2024) **144,** 1112−1123; doi:10.1016/j.jid.2023.10.026

INTRODUCTION

Ticks are ectoparasites that feed on blood from various vertebrate hosts and are vectors of a wide variety of pathogens with veterinary and medical importance (Rochlin and Toledo, 2020). They are blood pool feeders, meaning that they feed by lacerating small blood vessels located under the skin and ingesting blood directly from the wound (Bartíková et al, 2020). The tick feeding cycle can be divided into 3 main phases: the preparatory phase, when the tick attaches onto the host's skin, creating the feeding lesion; the slow feeding phase, during which the tick ingests moderate amounts of blood and begins to transmit pathogens through saliva; and the rapid feeding phase, when the tick feeds to repletion (Franta et al, 2010). Depending on the stage and the tick species, it might take several days for ticks to complete their blood-feeding process (Saraiva et al, 2014).

The feeding style utilized by ticks triggers several host-derived responses, and they face the challenge of wound healing, which is achieved through 4 precisely and highly programmed phases: hemostasis, inflammation, cell proliferation and migration, and remodeling (Qu and Chaikof, 2010), altogether representing barriers to the acquisition of a blood meal. To overcome these barriers, tick salivary glands have evolved a complex and sophisticated pharmacological armamentarium, consisting of bioactive molecules, to assist blood feeding. Tick saliva contains hundreds of compounds that have anticoagulant, vasodilatory, anti-inflammatory, and immunomodulatory functions, supporting the blood feeding (Ali et al, 2022; Francischetti et al, 2009). While helping the vector to feed, its saliva also modifies the site where pathogens are injected and, in many cases, facilitates the infection process (Nuttall, 2023).

The skin serves as the first host tissue that the tick mouthparts, tick saliva, and a tick-borne pathogen contact during

[1]*Tick-Pathogen Transmission Unit, Laboratory of Bacteriology, National Institute of Allergy and Infectious Diseases, Hamilton, Montana, USA;* [2]*Centro de Pesquisa Experimental, Hospital de Clínicas de Porto Alegre, Porto Alegre, Brazil;* [3]*Universidade Federal de Ciências da Saúde de Porto Alegre, Porto Alegre, Brazil;* [4]*Centro de Biotecnologia, Universidade Federal do Rio Grande do Sul, Porto Alegre, Brazil;* [5]*Laboratory of Infectious Diseases, Department of Disease Control, Graduate School of Veterinary Medicine, Hokkaido University, Sapporo, Japan;* [6]*Faculdade de Veterinária, Universidade Federal do Rio Grande do Sul, Porto Alegre, Brazil; and* [7]*Instituto Nacional de Ciência e Tecnologia-Entomologia Molecular, Rio de Janeiro, Brazil*

[8]*These authors contributed equally to this work.*

Correspondence: Lucas Tirloni, Rocky Mountain Laboratories, National Institute of Allergy and Infectious Diseases, National Institutes of Health, 903 South 4th Street, Hamilton, Montana 59840, USA. E-mail: lucas.tirloni@nih.gov and Adriana Seixas, Departamento de Farmacociências, Universidade Federal de Ciências da Saúde de Porto Alegre, Rua Sarmento Leite, 245, Porto Alegre 90050-170, Brazil. E-mail: adrianaseixas@ufcspa.edu.br

Abbreviations: ATIII, antithrombin III; KC, keratinocyte; PLG, plasminogen

Received 18 August 2023; revised 28 September 2023; accepted 10 October 2023; accepted manuscript published online 22 November 2023; corrected proof published online 12 January 2024

feeding. Consequently, tick saliva has evolved with various molecules capable of modulating wound healing (Bartíková et al, 2020). In this study, we characterized a Kunitz-type serine protease inhibitor obtained from *Ixodes persulcatus*, a tick species geographically distributed in Far East Asia and South Eurasia and known to be a vector for several human pathogens (Alekseev et al, 1999; Konnai et al, 2011; Randolph, 2008). Named persulcatin, this inhibitor effectively inhibits plasmin and thrombin, modulates keratinocyte (KC) migration, delays blood coagulation, and decreases endothelial cell permeability induced by thrombin. The biological functions of persulcatin unveil further insights into the intricate mechanisms governing wound healing and provide a fresh perspective on the intricate interactions between ticks and their host organisms.

RESULTS

Persulcatin is a Kunitz-type inhibitor of plasmin and thrombin isolated from *I persulcatus* ticks

The persulcatin cDNA consists of 438 bp, coding for a 145-amino acid protein, including a 15-amino acid signal peptide. Sequence and predicted structural analyses revealed the presence of 2 Kunitz-type domains containing 6 conserved cysteine residues, which are predicted to form 3 disulfide bonds per domain. The P1 residue, located in the inhibitory reactive site, is an arginine residue in the first domain and a lysine in the second domain (Figure 1a). Alignment with other tick proteins belonging to the Kunitz-type serine protease inhibitor family demonstrated conserved amino acid residues and similarity (Figure 1a). The phylogenetic tree constructed using sequences of Kunitz-type inhibitors from different species indicated that persulcatin is evolutionarily related to boophilin and hemalin, previously identified in *Rhipicephalus microplus* and *Haemaphysalis longicornis* ticks, respectively (Figure 1b). The predicted tertiary structure of persulcatin further confirmed the presence of the 2 inhibitory domains commonly found in Kunitz-type inhibitors (Figure 1c).

Persulcatin expression was examined in different tick stages and organs, suggesting its potential role in tick feeding. An increase in transcription was observed after blood feeding in larvae and nymphs. Adult females in the fed stage showed higher expression levels in the salivary gland, midgut, and ovary (Figure 1d).

Recombinant persulcatin was successfully expressed in human embryonic kidney 293 cells and subsequently purified using affinity, ion-exchange, and gel-filtration chromatography (Figure 1e). Protein homogeneity was confirmed by reducing SDS-PAGE, showing a single band at approximately 25 kDa (Figure 1e, inset). The specificity of persulcatin was verified in a screening assay optimized to detect protease inhibitors. Persulcatin blocks partially or entirely the amidolytic activity of α-thrombin, activated protein C, pancreatic chymotrypsin, plasmin, and pancreatic trypsin (Figure 1f). Because the screening with the peptide-derived amidolytic substrate for α-thrombin indicated a partial inhibition, we proceeded to confirm this activity using the macromolecular substrate, fibrinogen. As shown in Figure 1g, persulcatin (at 1 μM) inhibits over 80% of α-thrombin–clotting potential.

Persulcatin is a classical fast, tight-binding competitive inhibitor of plasmin

Progress curves demonstrated that plasmin inhibition occurs in a dose-dependent manner (Figure 2a). Preincubation time between the enzyme and inhibitor did not significantly change the progress curves behavior, suggesting that plasmin inhibition by persulcatin occurs in a fast-binding mode (Figure 2b). Plotting the fractional velocity as a function of persulcatin at different enzyme concentrations resulted in directly proportional half-maximal inhibitory concentration values, indicating that persulcatin is a tight-binding inhibitor for plasmin (Figure 2c). This tight-binding inhibition was confirmed by plotting the half-maximal inhibitory concentration values as a function of enzyme concentrations at a single fixed substrate concentration, yielding an apparent K_i (K_i^{app}) of 13 nM (Figure 2d). Considering that persulcatin is a tight binding inhibitor, the Morrison equation (Morrison, 1969) was used to fit fractional velocities as a function of inhibitor at different substrate concentrations (Figure 2e). The half-maximal inhibitory concentration values showed a linear relationship with substrate concentrations, indicating a competitive inhibition mode of action (Figure 2e, inset). In addition, the classical graphic method of Dixon (Dixon, 1953) for tight-binding competitive inhibitors was utilized to determine the real K_i, resulting in a K_i of 28 nM (Figure 2f).

Persulcatin inhibits KC migration induced by plasmin

The plasminogen (PLG)/plasmin system plays a crucial role in regulating pericellular proteolysis events involved in cell migration and wound healing (Li et al, 2003). To investigate whether KC surfaces can generate active plasmin, triggering cell migration, we conducted experiments as shown in Supplementary Figure S1. The results demonstrate that PLG dose-dependently accelerates KC migration in the scratch-induced assay (Supplementary Figure S1a and b). Furthermore, active plasmin was also generated on KC surface after the addition of PLG, showing a dose (Supplementary Figure S1c) and time (Supplementary Figure S1d) -dependent manner.

We present evidence that persulcatin hinders PLG/plasmin-induced KC migration (Figure 3 and Supplementary Figure S2). The scratch-induced assay revealed reduced KC migration in PLG-stimulated cells in the presence of persulcatin (Figure 3a and b). In addition, persulcatin-treated cells generated less active plasmin, as detected in the conditioned culture media obtained from KCs (Figure 3c). This observation was further confirmed by zymography using fibrin as substrate (Figure 3d) and fibrin clot degradation assays (Figure 3e), where persulcatin clearly blocked fibrin degradation induced by formed plasmin. Moreover, persulcatin downregulated matrix metalloproteinase 2 and matrix metalloproteinase 9 secretion (Figure 3f and g) and inhibited fibronectin (Figure 3h) and collagen type 1A (Figure 3i) degradation in KC-conditioned media. These findings suggest that the inhibitory effects of persulcatin on the PLG/plasmin system may play a critical role in modulating KC migration and proteolysis during the wound-healing process.

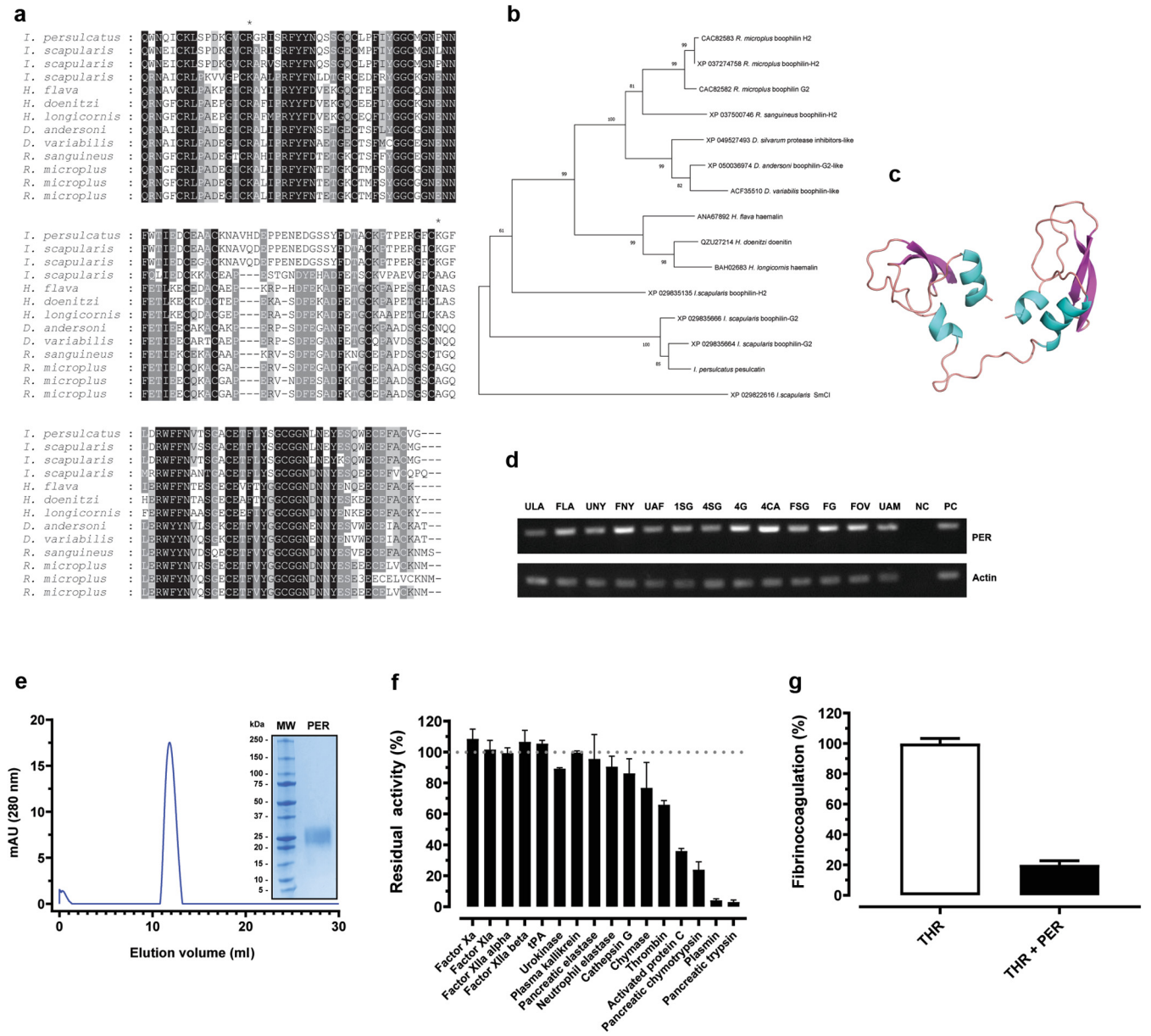

Figure 1. PER is a Kunitz-type inhibitor of plasmin and thrombin isolated from *Ixodes persulcatus* ticks. (**a**) MUSCLE alignment of PER (accession number OQ067579) and other similar sequences (XP_029835664 *Ixodes scapularis* boophilin-G2, XP_029835666 *Ixodes scapularis* boophilin-G2, XP_050036974 *Dermacentor andersoni* boophilin-G2 like, ANA67892 *Haemaphysalis flava* haemalin, CAC82582 *Rhipicephalus microplus* boophilin G2, CAC82583 *Rhipicephalus microplus* boophilin H2, ACF35510 *Dermacentor variabilis* boophilin like, QZU27214 *Haemaphysalis doenitzi* doenitin, XP_037274758 *Rhipicephalus microplus* boophilin-H2, XP_029835135 *Ixodes scapularis* boophilin-H2, XP_049527493 *Dermacentor silvarum* protease inhibitors like, XP_037500746 *Rhipicephalus sanguineus* boophilin-H2, BAH02683 *Haemaphysalis longicornis* haemalin, and XP_02982261 *Ixodes scapularis* carboxypeptidase inhibitor SmCI). Conserved amino acid residues are highlighted in black to gray scale. The P1 residue of each Kunitz-type domain is indicated by an asterisk. (**b**) Phylogram of PER and other tick similar sequences (accession numbers described earlier). (**c**) Structure of PER predicted by AlphaFold2 and visualized using PyMol; β-sheet domains are highlighted in magenta, and α-helixes are highlighted in cyan. Regions comprising the 2 Kunitz-type domains were modeled with pLDDT > 90 and are expected to have high accuracy. Regions with pLDDT < 80 were identified within flexible loops, including the first 4 residues at the N-terminus, the last residue at the C-terminus, and the flexible loop between the 2 domains, which is a strong predictor of disorder, as expected for flexible loops. (**d**) RT-PCR showing the transcriptional profile of PER (denoted as PER) in different tick stages and organs: unfed larvae (denoted as ULA), fed larvae (denoted as FLA), unfed nymphs (denoted as UNY), fed nymphs (denoted as FNY), unfed adult female (denoted as UAF), 1-day fed adult female salivary gland (denoted as 1SG), 4-day fed adult female salivary gland (denoted as 4SG), 4-day fed adult female midgut (denoted as 4G), 4-day fed adult female carcass (denoted as 4CA), fully fed adult female salivary gland (denoted asFSG), fully fed adult female midgut (denoted as FG), fully fed adult female ovary (denoted as FOV), unfed adult male (denoted as UAM), negative control (denoted as NC), and positive control (denoted as PC). (**e**) A chromatogram obtained from a Superdex 75 column run exhibits a single peak corresponding to purified PER . The insert presents PER solved in an SDS-PAGE under reducing conditions, stained with Coomassie blue. (**f**) Inhibitory activity of PER (1 μM) against different host-derived proteases. (**g**) Inhibition of α-thrombin (denoted as THR)–induced fibrinogen coagulation by PER (1 μM). MUSCLE, multiple sequence comparison by log- expectation; MW, molecular weight; PER, persulcatin; pLDDT, predicted local distance difference test.

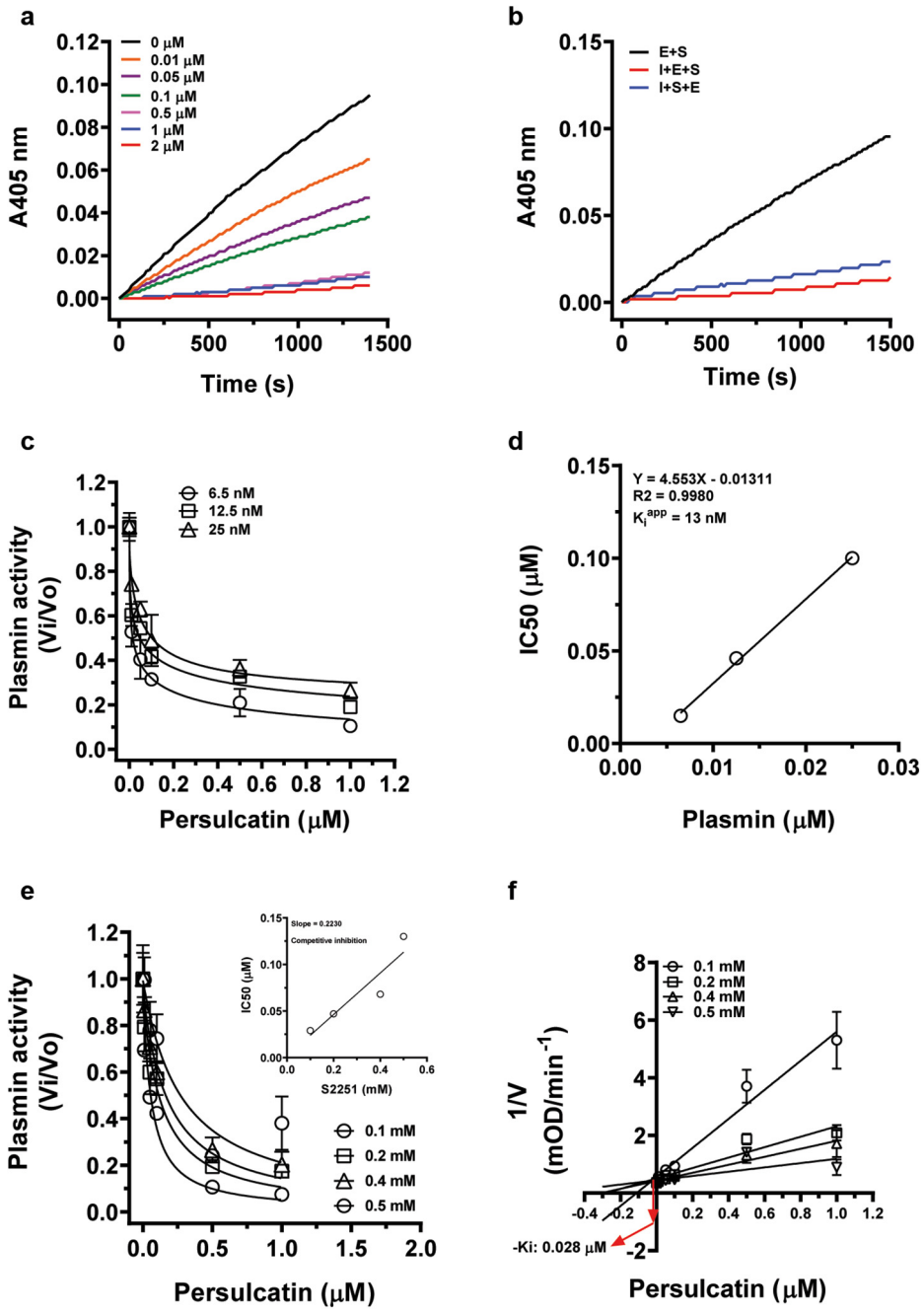

Figure 2. Persulcatin is a competitive and tight-binding inhibitor of plasmin. (**a**) Progress curves displaying plasmin-mediated S-2251 hydrolysis with varying persulcatin concentrations (0–2 µM). (**b**) Plasmin-catalyzed hydrolysis of S-2251 was analyzed before (I+S+E) and after (I+E+S) previous incubation (45 min) with persulcatin (500 nM). Plasmin (denoted as E), persulcatin (denoted as I), and S-2251 (denoted as S). (**c**) Dose–response plot of fractional velocity (Vi/Vo) as a function of persulcatin (0–1 µM) at different plasmin concentrations (6.5, 12.5, and 25 nM). (**d**) Linear behavior of IC_{50} values as a function of plasmin concentration indicating a tight-binding mode of inhibition by persulcatin and its apparent K_i (K_i^{app}). (**e**) Morrison's plot as a function of persulcatin (0–1 µM) at different S-2251 concentrations (0.1, 0.2, 0.4, and 0.5 mM), indicating a competitive inhibition. (**f**) Typical Dixon's plot as a function of persulcatin at different S-2251 concentrations (0.1, 0.2, 0.4, and 0.5 mM) to determine the real K_i value. IC_{50}, half-maximal inhibitory concentration; min, minute; s, second.

Persulcatin binds to exosite-1 of thrombin, impairing blood coagulation and endothelial cell permeability

Once persulcatin also targets α-thrombin, we proceeded with its characterization on blood coagulation. Persulcatin significantly delayed the human plasma recalcification time (Figure 4a) and prolonged activated partial thromboplastin time (Figure 4b) and prothrombin time (Figure 4c), confirming its function as an inhibitor of the common pathway of blood coagulation. In a cell-based coagulation assay, persulcatin prolonged the coagulation time measured directly on the surface of lipopolysaccharide-activated endothelial cells (Figure 4d) and significantly inhibited the ex vivo thrombin-induced tissue factor protein expression in mouse aortic rings (Figure 4e).

The mechanism of α-thrombin inhibition by persulcatin using fibrinogen as the substrate is elucidated in Figure 5a–f. Progress curves demonstrated the impact of persulcatin on α-thrombin–mediated fibrinogen coagulation (Figure 5a). Similar to plasmin, thrombin inhibition by persulcatin was not time dependent, occurring in a fast-binding mode (Figure 5b). Persulcatin tightly binds to α-thrombin, as indicated by dose–response plots (Figure 5c) and half-maximal inhibitory concentration (Figure 5d) analyses. The competitive inhibition mechanism was confirmed by Morrison's

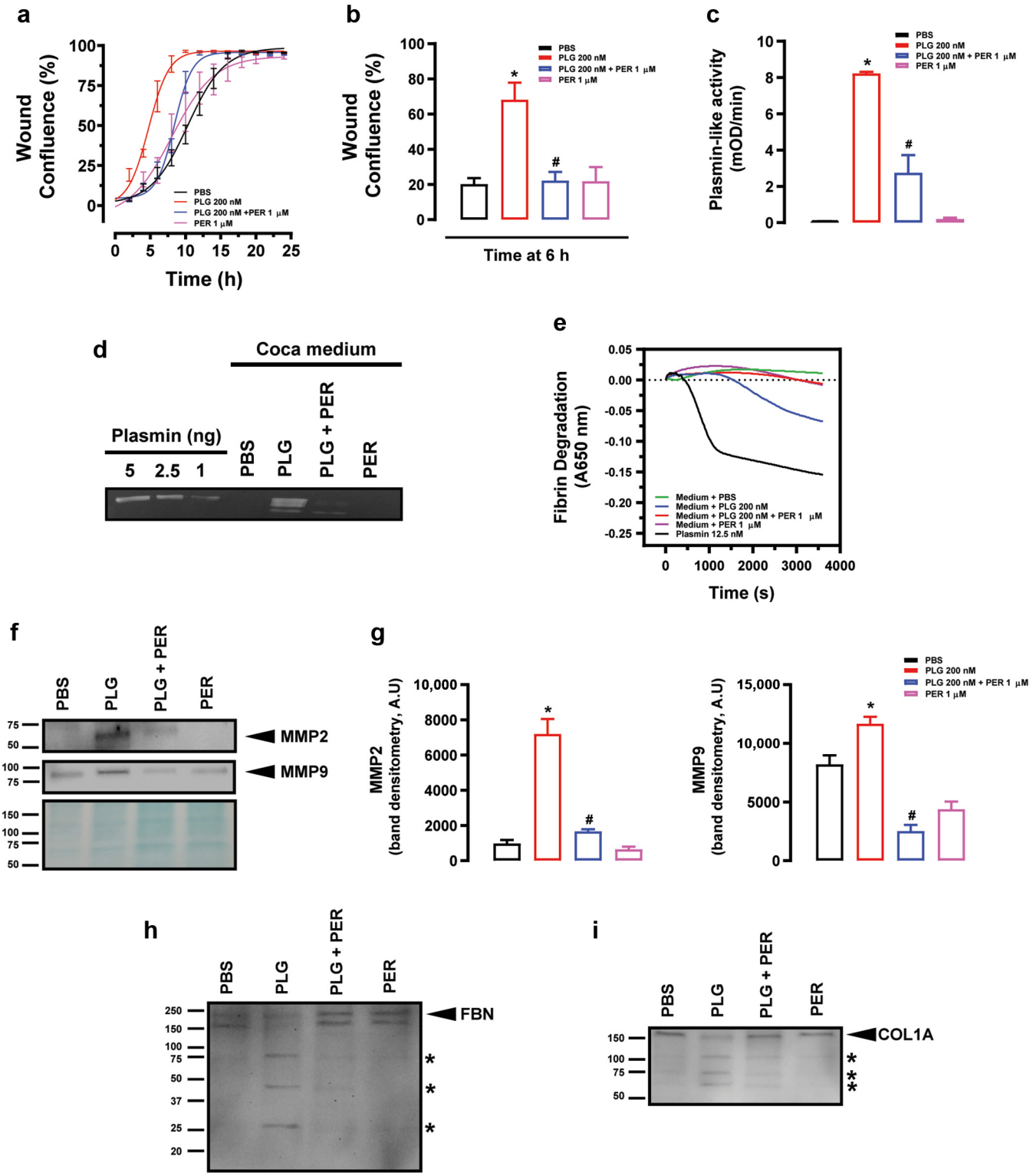

Figure 3. PER inhibits PLG/plasmin-induced keratinocyte migration. (**a**) The migration of keratinocytes (COCA cell line) was assessed over a 24-hour period using the classical scratch-induced wound-healing assay in cell monolayers. The assay was conducted in the presence of PBS, PLG (200 nM), and/or PER (1 µM). The assessment was based on the percentage of wound confluence. (**b**) After inducing a scratch in the keratinocyte monolayer, quantitative analysis was performed to measure migration after 6 hours. Administration of PBS, PLG (200 nM), and/or PER (1 µM) was considered in the assessment. (**c**) Plasmin-like activity generated in the keratinocyte-conditioned media as estimated on the basis of S-2251 hydrolysis. (**d**) Plasmin generation in the keratinocyte-conditioned media as estimated by zymography using fibrin as substrate. (**e**) Progress curves for plasmin-like activity generated in the keratinocyte-conditioned media as estimated on the basis of direct measurement of fibrin degradation. (**f**) Immunoblots for MMP2 and MMP9 in the keratinocyte-conditioned media. (**g**) Quantitative analyses for MMP2 and MMP9 detected in keratinocyte-conditioned media. (**h**) Fibronectin and (**i**) collagen type 1A degradation pattern in the keratinocyte-conditioned media was estimated by immunoblot. The asterisk shows degradation bands formed by generated plasmin. The data represent mean ± SE. *$P < .05$ versus PBS and #$P < .05$ versus PLG 200 nM group. MMP, matrix metalloproteinase; PER, persulcatin; PLG, plasminogen; SE, standard error.

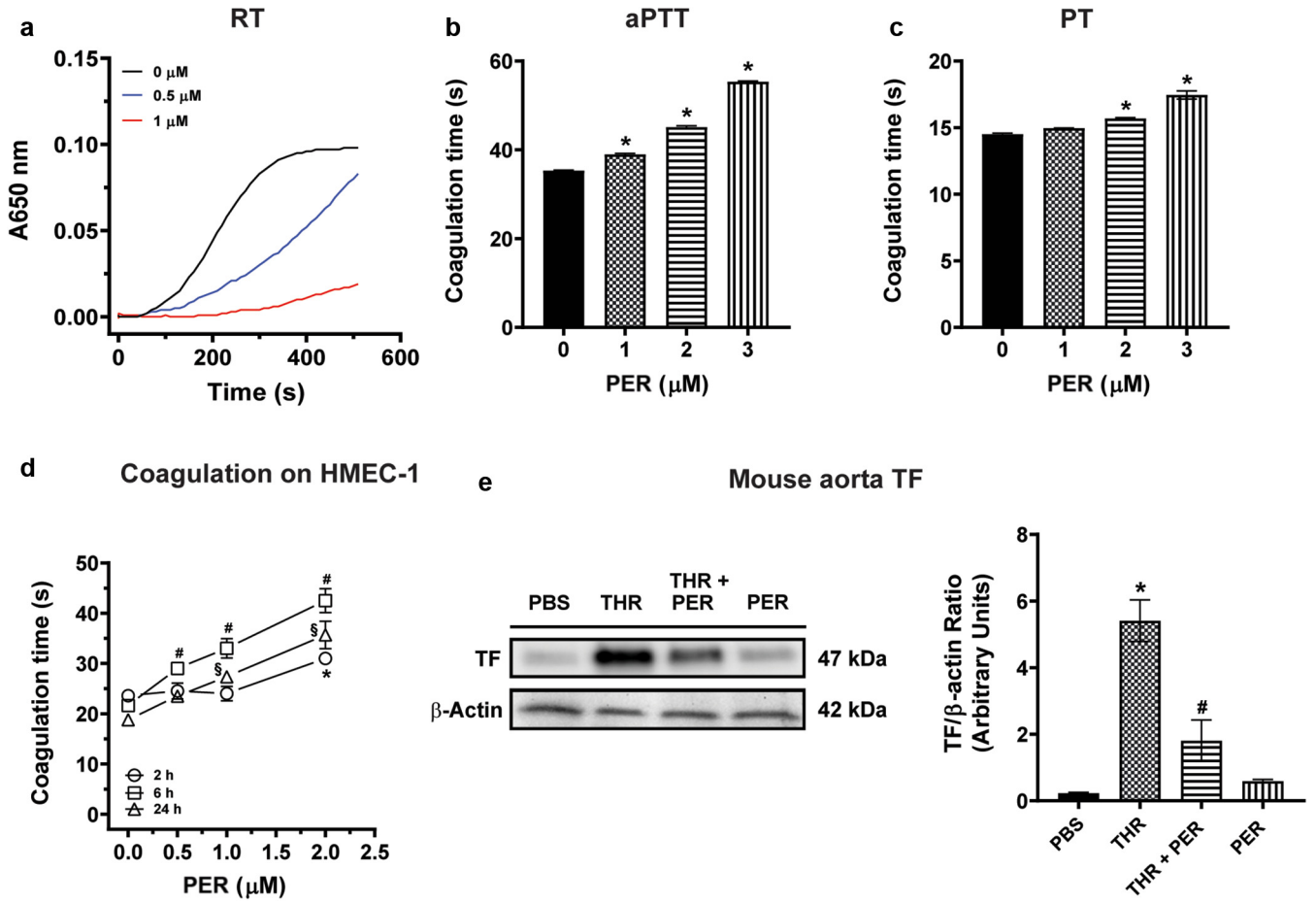

Figure 4. PER inhibits blood coagulation. (**a**) Typical progress curves for human plasma RT assay in the absence or presence (0−1 μM) of PER. (**b**) aPTT and (**c**) PT assays were measured in vitro after incubation with PER (0−3 μM). *$P < .05$ versus PER at 0 μM. (**d**) Human endothelial cells (HMEC-1 cell line) were preactivated with LPS by 2, 6, and 24 h. Then, the coagulation time was estimated on cell surface by the addition of human plasma containing PER (0−2 μM). *$P < .05$ versus PER at 0 μM (2 h group), #$P < .05$ versus PER at 0 μM (6 h group), and §$P < .05$ versus PER at 0 μM (24 h group). (**e**) Immunoblot showing α-thrombin (denoted as THR)−induced TF protein expression in mouse aortic rings previously incubated ex vivo with 25 nM THR and/or 1 μM PER. All presented data represent mean ± SE. aPTT, activated partial thromboplastin time; h, hour; HMEC-1, human microvascular endothelial cell 1; LPS, lipopolysaccharide; PER, persulcatin; PT, prothrombin time; RT, recalcification time; SE, standard error; TF, tissue factor.

(Figure 5e) and Dixon's (Figure 5f) plots, resulting in a K_i value of 115 nM.

Considering that α-thrombin interactions with its natural substrates and other tick-derived inhibitors happen mainly through binding to the active site and/or to the anion-binding exosites (Alexander et al, 2012; Corral-Rodríguez et al, 2009), we employed a biochemical approach to study the preferred site for persulcatin (Figure 5g−l). Comparing the dose−response inhibition curves, persulcatin displayed behavior similar to that of hirudin, an inhibitor that exclusively binds to the exosite-1 of α-thrombin (Fenton et al, 1991). Persulcatin had inhibitory effects when the macromolecular substrate fibrinogen was used (Figure 5g) but had minor or no effects in the presence of the small peptide-based synthetic substrate S-2238 (Figure 5h). Similarly, persulcatin did not change the exosite-1−deleted γ-thrombin activity upon S-2338, suggesting an important role for this domain (Figure 5i). The interaction with exosite-1 was confirmed by bivalirudin and antithrombin III (ATIII) displacement experiments. Bivalirudin is a synthetic peptide-derived inhibitor engineered to interact with both the active site and exosite-1 simultaneously, whereas ATIII is a physiological macromolecular inhibitor able to interact with the active site but susceptible to allosteric modulations at the exosite-1 (Trapaidze et al, 2016). Increasing concentrations of persulcatin caused the displacement of bivalirudin (Figure 5j) and ATIII (Figure 5k), significantly reducing their α-thrombin inhibitory potential upon S-2238 hydrolysis. Figure 5l shows the molecular surface of persulcatin according to its electrostatic potential. Highlighted in red are the negatively charged patches composed of the residues that can potentially interact with the anion-binding exosite-1.

Endothelial cell barrier and permeability at the capillary vessel−tissue interface can be modulated and even disrupted by proteases (Claesson-Welsh et al, 2021). Figure 6 shows cases that α-thrombin increases endothelial cell permeability to FITC-dextran (Figure 6a) by disrupting vascular endothelial-cadherin and cell−cell contacts (Figure 6b). On the other hand, endothelial cells pretreated with persulcatin revealed reduced permeability when stimulated with α-thrombin, and vascular endothelial-cadherin immunostaining confirmed the modulatory effects of persulcatin.

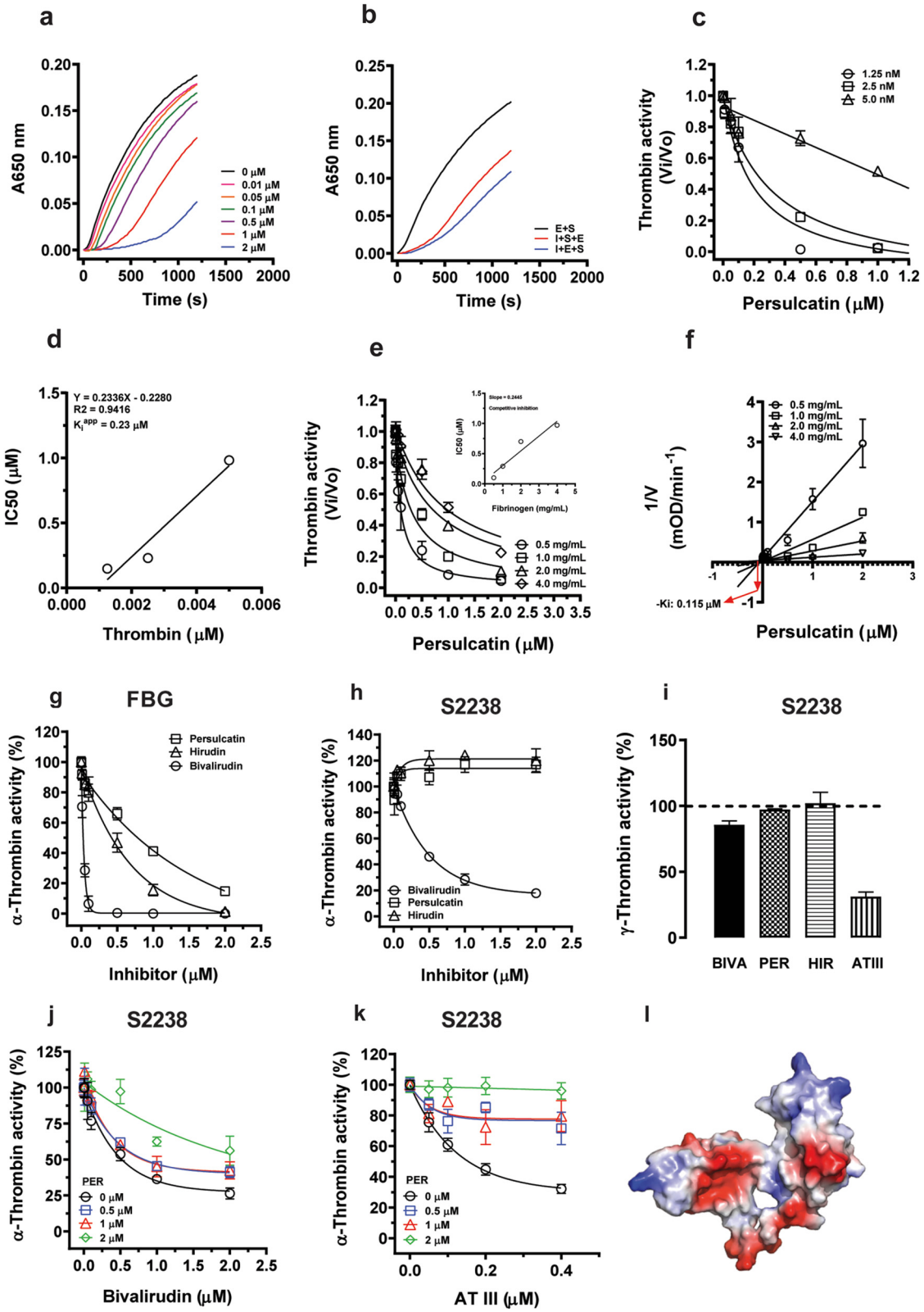

Figure 5. Mechanism of α-thrombin inhibition by persulcatin. (**a**) Progress curves for α-thrombin–mediated FBG coagulation in the absence and presence of persulcatin (0–2 µM). (**b**) α-Thrombin–induced FBG coagulation was analyzed before (I+S+E) and after (I+E+S) previous incubation (45 min) with persulcatin (500 nM). α-Thrombin (denoted as E), persulcatin (denoted as I), and FBG (denoted as S). (**c**) Dose–response plot of fractional velocity (Vi/Vo) as a function of persulcatin (0–1 µM) at different α-thrombin concentrations (1.25, 2.5, and 5.0 nM). (**d**) Linear behavior of IC_{50} values as a function of α-thrombin concentration indicating a tight-binding mode of inhibition by persulcatin and its apparent K_i (K_i^{app}). (**e**) Morrison's plot as a function of persulcatin (0–2 µM) at different FBG concentrations (0.5, 1.0, 2.0, and 4.0 mM). The insert shows a positive correlation between IC_{50} values and substrate concentrations indicating a competitive inhibition. (**f**) Typical Dixon's plot as a function of persulcatin at different FBG concentrations to determine the real K_i value. (**g**) α-Thrombin–induced FBG coagulation, (**h**) α-Thrombin–mediated S-2238 hydrolysis, and (**i**) γ-Thrombin–mediated S-2238 hydrolysis in the presence of

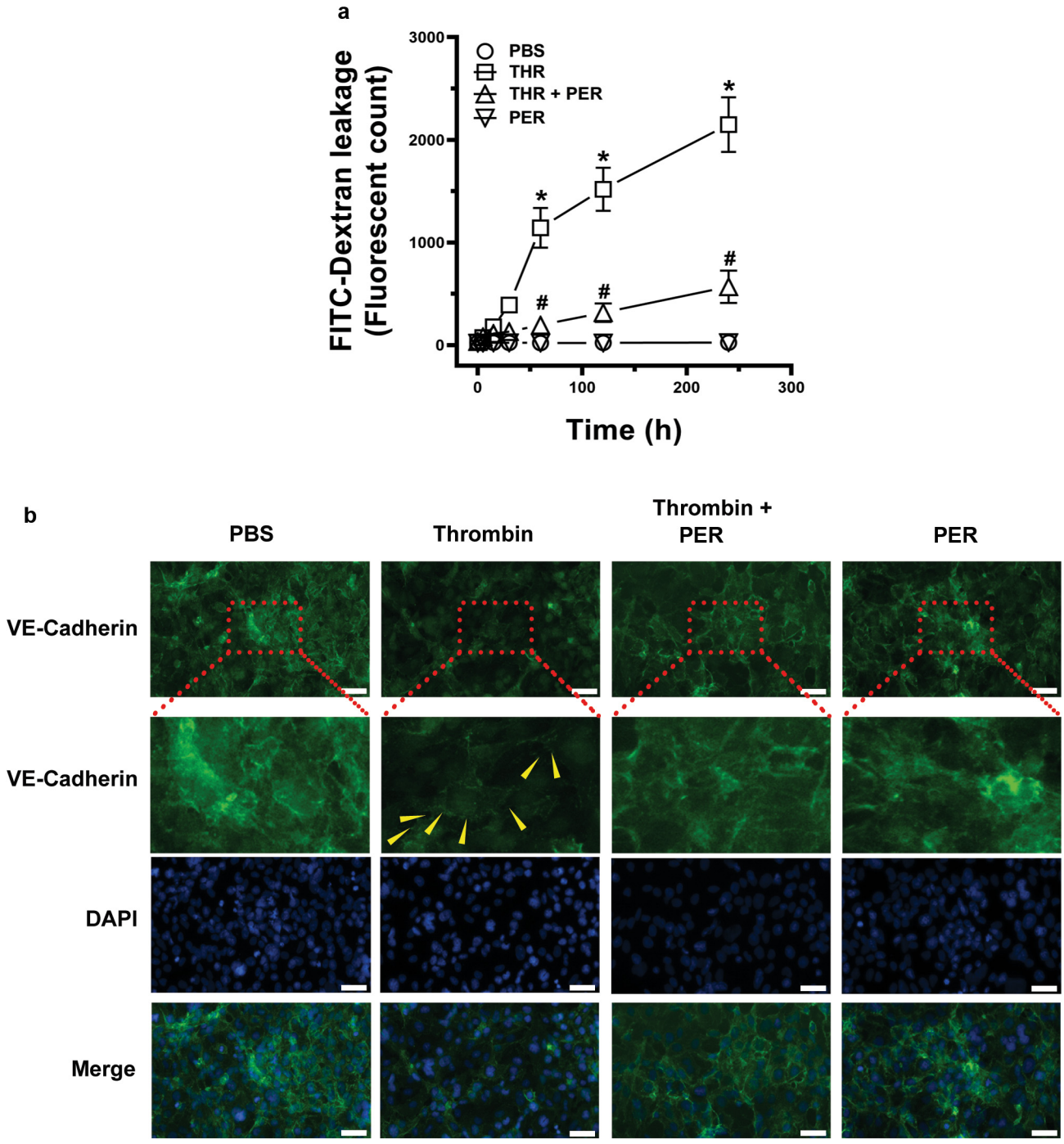

Figure 6. PER inhibits thrombin-induced endothelial cell permeability. (**a**) FITC-dextran assay was used to measure endothelial cell monolayer permeability (HMEC-1 cell line). The fluorescence intensity was quantified at different time points (0–4 h) after HMEC-1 treatment with PBS, 50 nM α-thrombin (denoted as THR), and/or 1 μM PER. *$P < .05$ versus PBS and #$P < .05$ versus THR. (**b**) Immunostaining for VE-cadherin on HMEC-1 surface after 1 h treatment with PBS, 50 nM THR, and/or 1 μM PER. The yellow arrowheads pointed to membrane gap formations, indicating VE-cadherin degradation. h, hour; HMEC-1, human microvascular endothelial cell 1; PER, persulcatin; VE, vascular endothelial.

DISCUSSION

Ticks, as ectoparasites and blood pool feeders, evolved to produce molecules in their saliva that exhibit high-affinity binding and specificity toward various components involved in skin physiology and wound healing (Ali et al, 2022). In this study, we present a detailed description of a

bivalirudin (denoted as BIVA), PER, hirudin (denoted as HIR), and ATIII. (**j**) Bivalirudin and (**k**) ATIII displacement from the α-thrombin interaction caused by increasing doses of PER (0, 0.5, 1.0, and 2.0 μM). (**l**) Electrostatic potential surface of persulcatin showing the neutral (white), positively (blue), and negatively (red) charged areas. All presented data represent mean ± SE. PER denotes persulcatin. ATIII, antithrombin III; FBG, fibrinogen; IC50, half-maximal inhibitory concentration; min, minute; SE, standard error.

tick salivary protein named persulcatin, isolated from *I persulcatus*, the primary vector of tick-borne encephalitis and Lyme disease in East Asia (Wu et al, 2013). Persulcatin demonstrates multifunctional properties as a Kunitz-type protease inhibitor, influencing host plasmin–induced cell migration on KCs and prothrombotic events mediated by thrombin on endothelial cells.

The skin epidermis serves as the initial point of contact for tick mouthparts, tick saliva, and tick-borne pathogens during the feeding process. This interface plays a critical role in influencing the host's initial response to tick feeding and pathogen transmission (Wikel, 2013). Of particular interest are KCs, because they constitute the majority of cells in the skin, playing a crucial role in skin homeostasis and rapidly responding to mechanical damage by secreting soluble factors such as cytokines, chemokines, proteases, and GFs, which are permanently involved in the crosstalk with immune cells (Bourke et al, 2015). The role of KCs is somehow a neglected topic in the context of tick feeding and tick-borne pathogen transmission biology.

KCs express various components of proteolytic systems, including elements of the PLG–plasmin system, such as PLG-binding proteins, urokinase-type PLG activator, and matriptase (Chen et al, 2016; Jaiswal et al, 2018). These components play vital roles in maintaining the structural integrity and barrier function of the epidermis (Chen et al, 2016; Jennemann et al, 2007). KC migration is a fundamental process in wound healing and tissue remodeling, allowing cells to move into the wound bed and facilitate the formation of new tissue (Seeger and Paller, 2015). Plasmin is not only essential for dissolving fibrin clots and removing necrotic tissue during KC migration in wound healing but also contributes to KC and inflammatory cell migration by activating and releasing GFs, activating matrix metalloproteases, promoting angiogenesis, and facilitating extracellular matrix remodeling (Deryugina and Quigley, 2012). Plasmin is initially synthesized and secreted as an inactive precursor, PLG, which is subsequently cleaved and activated by soluble tissue type-PLG activator, membrane-associated urokinase-type PLG activator, and/or matriptase, resulting in the generation of active plasmin (Chen et al, 2016; Lund et al, 2006). Therefore, the regulation of the PLG–plasmin system serves critical roles at every stage of the wound-healing process, and any disruption in this system can have significant impacts on the process. Persulcatin functions as a classical fast, tight-binding competitive inhibitor, targeting plasmin with a K_i value of 28 nM. Notably, persulcatin appears to operate as a down-modulator of the PLG–plasmin system, effectively inhibiting the activation of PLG and consequent generation of plasmin on KCs. This inhibition consequently leads to the reduction in the migratory ability of KCs rather than affecting cell proliferation because plasmin apparently does not promote cell proliferation in KCs (Szabo et al, 2004). Beyond its direct influence on plasmin, persulcatin takes on the additional role of downregulating matrix metalloproteinase expression within KCs, resulting in a decrease in their capacity to degrade essential extracellular matrix proteins, such as fibronectin, fibrin, or collagen 1A. This dual-pronged mechanism highlights how persulcatin orchestrates a complex regulatory milieu, curtailing the signaling pathways that typically encourage KC migration into the wound bed. Therefore, the presence of persulcatin in tick saliva can inhibit the signaling that promotes KC migration into the wound bed, making tissue damage repair more difficult, while simultaneously facilitating blood meal acquisition (Pham et al, 2021). This highlights the importance of characterizing persulcatin and understanding its functional effects on KCs.

Besides healing mechanisms, hemostasis is another host-derived response that occurs locally at the bite site (Chmelar et al, 2012). Ticks have evolved to produce salivary molecules that counteract specific targets involved in vasoconstriction, platelet aggregation, and the coagulation cascade (Tirloni et al, 2020, 2016, 2014). These molecules include inhibitors of clotting factors such as factors Xa, XIIa, XIa, and IXa; thrombin; tissue factor/VIIa; and plasma kallikrein (Parizi et al, 2018). An example of such tick salivary inhibitors is persulcatin, which in addition to its role in targeting plasmin and KC migration targets α-thrombin, inhibiting its ability to clot fibrinogen competitively with a K_i of 115 nM. As a result, persulcatin prolongs classic coagulation time parameters in human plasma, inhibits coagulation in lipopolysaccharide-activated endothelial cells, and downregulates tissue factor expression in mice aorta. From a molecular standpoint, persulcatin features 2 Kunitz-like domains, containing 6 cysteine residues per domain. It shares structural similarities with other tick thrombin inhibitors such as hemalin from *H longicornis* (Liao et al, 2009), amblin from *Amblyomma hebraeum* (Lai et al, 2004), and boophilin from *R microplus* (Macedo-Ribeiro et al, 2008; Soares et al, 2012). Persulcatin is evolutionary closely related to boophilin, a 2 Kunitz-type inhibitor derived from *R microplus* midgut, previously characterized as an anticoagulant and antithrombotic molecule (Assumpção et al, 2016). Unlike boophilin, which behaves as a noncompetitive α-thrombin inhibitor interacting with both catalytic site and exosite-1 (Assumpção et al, 2016), persulcatin is a competitive inhibitor that seems to exclusively interact with α-thrombin exosite-1. The function of α-thrombin depends on its active site and 2 anion-binding exosites that mediate enzyme interaction with various macromolecular substrates and inhibitors (Krishnaswamy, 2005). Exosite-1 binds to fibrinogen, PAR-1 receptor, thrombomodulin, heparin cofactor II, and factors V/Va, whereas exosite-2 is the heparin-binding site (Abdel Aziz and Desai, 2018). Inhibitors binding to exosite-1 can physically obstruct macromolecular substrate recognition or induce allosteric changes in the catalytic site. Consequently, the ability of the enzyme to cleave small synthetic peptide substrates could remain partially unchanged, but its activity against macromolecular substrates, such as fibrinogen, is severely impaired (Grzegorski et al, 2020). This phenomenon is observed with persulcatin and hirudin, both pure exosite-1 inhibitors. These inhibitors do not block S-2238 hydrolysis but exhibit potent anticoagulant effects. At a 500-fold ratio to α-thrombin, persulcatin inhibits around 30% of the S-2238 hydrolysis by α-thrombin. Notably, persulcatin binding to exosite-1 also appears to induce allosteric changes that protect thrombin from serpin inactivation, as indicated by the ATIII displacement experiments. Although ATIII recognition by thrombin does not directly rely on exosite-1 interaction,

ligand binding or inactivation of exosite-1 can allosterically reduce catalytic site inactivation by ATIII (Lane et al, 2005).

Beyond its role in blood coagulation, thrombin activates the PAR-1 receptor in endothelial cells, initiating downstream pathways of phosphoinositide 3-kinase/protein kinase B pathway, MAPK pathway, and the Rho GTPase pathway (Zohrabian et al, 2009). Thrombin-induced Rho GTPase activation triggers actin cytoskeleton reorganization and stress fiber formation, leading to endothelial cell contraction and barrier disruption (Yang and Chen, 2022). Our data indicate that thrombin disrupts vascular endothelial-cadherin in endothelial cells, inducing cell contraction, increasing intercellular space, and enhancing cell permeability to FITC-dextran. Persulcatin counteracts thrombin-induced endothelial cell permeability, preserving vascular endothelial-cadherin structural integrity. Given that increased vascular permeability is essential for primary inflammatory responses and inflammatory cell migration, persulcatin likely contributes to tick feeding process by safeguarding endothelial cell tight junctions from proteases activity.

In conclusion, this study elucidates the multifunctional properties of persulcatin, a molecule discovered in the salivary glands of *I persulcatus* ticks. By inhibiting plasmin-induced cell migration on KCs and thrombin-associated prothrombotic events in endothelial cells, persulcatin effectively regulates KC migration, blood coagulation, endothelial cell permeability, and extracellular matrix function. This ultimately aids in the tick feeding process. The findings underscore the pivotal role persulcatin plays in modulating the initial host response during tick feeding, facilitating successful blood meals, and potentially assisting in the transmission of tick-borne pathogens. This discovery deepens our comprehension of the intricate interactions among ticks, their saliva, and the host, offering valuable insights for future research and potential applications in combating tick-borne diseases.

MATERIALS AND METHODS

Animals and ethics statement

I persulcatus ticks used in all experiments were obtained from laboratory colonies maintained using Syrian hamsters as hosts (Japan SLC, Shizuoka, Japan) in an isolated experimental animal facility of the Graduate School of Veterinary Medicine, Hokkaido University (Sapporo, Japan), following the standard procedures for tick colony maintenance and management (Konnai et al, 2008). The protocols for all experiments involving animals and ticks were approved by the Ethics Committee of the Faculty of Veterinary Medicine, Hokkaido University (22-0035). C57BL/6J mice were purchased from Charles River Laboratories and used for the ex vivo aortic ring assays (details are provided in the Supplementary Materials and Methods). The animals were kept under the care of the Rocky Mountain Veterinary Branch at the Rocky Mountain Laboratories (Hamilton, MT). The National Institutes of Health Guide for the Care and Use of Laboratory Animals was followed in all the procedures, and collection of mice tissue was approved by the Animal Care and Use Committee at the Rocky Mountain Laboratories (2020-045).

Protein expression, purification, and characterization

Bioinformatic analyses were employed to characterize the sequence alignment, phylogeny, and specific structural aspects of persulcatin in comparison with those of other Kunitz-type inhibitors. The protein-coding sequence corresponding to mature persulcatin was cloned and further optimized for mammalian expression using Expi293 human embryonic kidney cells (Thermo Fisher Scientific, Waltham, MA). Subsequently, the recombinant protein was purified, employing conventional protein purification chromatography methods. The specificity of persulcatin was assessed through a comprehensive broad panel of proteases crucial for coagulation, inflammation, and immune response against tick feeding. Further details of these experiments can be found in the Supplementary Materials and Methods.

Protease and blood coagulation experiments

In-depth investigation was carried out on the effects of persulcatin against human plasmin and α-thrombin to characterize the mechanisms of inhibition, kinetics, mode of action, and binding aspects within protease−inhibitor interactions. The ability of persulcatin to modulate blood coagulation was explored through the following approaches: (i) measurement of coagulation time parameters in human plasma, (ii) assessment of clot formation on the surface of lipopolysaccharide-activated endothelial cells, and (iii) evaluation of thrombin-induced tissue factor expression in ex vivo aortic rings. Detailed procedures for these experiments can be found in the Supplementary Materials and Methods.

Cellular and molecular analyses

The scratch-induced wound healing assay was employed on KC monolayers to estimate cell migration and to explore the mechanisms of PLG/plasmin system modulation by persulcatin. The analysis encompassed cell surface plasmin generation, matrix metalloproteinase activation, as well as fibrin and matrix protein degradation. Endothelial cell monolayers were used to investigate the effects of persulcatin on thrombin-induced cell permeability and tight junction protein degradation. Detailed procedures for these and other experiments (immunofluorescence, western blot, and RT-PCR) can be found in Supplementary Materials and Methods.

Data analyses

Data analyses were conducted using GraphPad Prism software (GraphPad Software, San Diego, CA). All data are presented as the means ± standard error of at least 3 replicates. Significance of differences was assessed by 1-way ANOVA, followed by unpaired *t*-tests with Bonferroni's correction for multiple comparisons. A significance level of $P < .05$ was considered statistically significant.

DATA AVAILABILITY STATEMENT

No datasets were generated or analyzed during this study.

ORCIDs

Markus Berger: http://orcid.org/0000-0001-7670-2584
Sheila Rosa da Mata: http://orcid.org/0000-0001-7769-4467
Nicolle Masseroni Pizzolatti: http://orcid.org/0009-0005-8993-5877
Luís Fernando Parizi: http://orcid.org/0000-0003-4652-7425
Satoru Konnai: http://orcid.org/0000-0002-3230-7109
Itabajara da Silva Vaz Jr: http://orcid.org/0000-0003-0309-9328
Adriana Seixas: http://orcid.org/0000-0003-1334-194X
Lucas Tirloni: http://orcid.org/0000-0003-4582-7100

CONFLICT OF INTEREST

The authors state no conflict of interest.

ACKNOWLEDGMENTS

This work utilized the computational resources of the National Institutes of Health High-Performance Computing Services Biowulf cluster (http://hpc.nih.gov). LT and MB were supported by the Intramural Research Program of the National Institute of Allergy and Infectious Diseases (Z01 AI001337-01). This research was supported by Japan Society for the Promotion of Science Grants-

in-Aid for Scientific Research (22H02503), Japan Agency for Medical Research and Development (JP19fk0108068), Conselho Nacional de Desenvolvimento Científico e Tecnológico (CNPq) (159522/2019-6, 405763/2018-2, 405799/2018-7 and 465678/2014-9 "INCT-EM - Instituto Nacional de Ciência e Tecnologia de Entomologia Molecular"), Coordenação de Aperfeiçoamento de Pessoal de Nível Superior (CAPES) (88882.346657/2019-01), Fundação de Amparo à Pesquisa do Estado do Rio Grande do Sul (FAPERGS) (21/2551-0002221-3), and Universidade Federal de Ciências da Saúde de Porto Alegre (UFCSPA) (Edital nº 01/2019/PROPPG-UFCSPA). We would like to acknowledge Ryan Kissinger and Anita Mora from the Visual and Medical Arts branch (Research Technologies Branch, National Institute of Allergy and Infectious Diseases, National Institutes of Health) for graphical abstract preparation. LT is designated as the guarantor for this study.

AUTHOR CONTRIBUTIONS

Conceptualization: MB, SRdM, NMP, IdSVj, AS, LT; Investigation: MB, SRdM, NMP, AS, LT; Funding Acquisition: SK, IdSVj, AS, LT; Writing - Original Draft Preparation: MB, SRM, IdSVj, AS, LT; Writing — Review and Editing: MB, SRdM, NMP, LFP, SK, IdSVj, AS, LT

SUPPLEMENTARY MATERIAL

Supplementary material is linked to the online version of the paper at www.jidonline.org, and at https://doi.org/10.1016/j.jid.2023.10.026.

REFERENCES

Abdel Aziz MH, Desai UR. Novel heparin mimetics reveal cooperativity between exosite 2 and sodium-binding site of thrombin. Thromb Res 2018;165:61–7.

Alekseev AN, Dubinina HV, Rijpkema SG, Schouls LM. Sexual transmission of *Borrelia garinii* by male *Ixodes persulcatus* ticks (Acari, Ixodidae). Exp Appl Acarol 1999;23:165–9.

Alexander KS, Fried MG, Farrell DH. Role of electrostatic interactions in binding of thrombin to the fibrinogen γ′ chain. Biochemistry 2012;51:3445–50.

Ali A, Zeb I, Alouffi A, Zahid H, Almutairi MM, Ayed Alshammari F, et al. Host Immune Responses to Salivary Components – a critical facet of tick-host interactions. Front Cell Infect Microbiol 2022;12:809052.

Assumpção TC, Ma D, Mizurini DM, Kini RM, Ribeiro JM, Kotsyfakis M, et al. In vitro mode of action and anti-thrombotic activity of Boophilin, a multifunctional Kunitz protease inhibitor from the midgut of a tick vector of babesiosis, *Rhipicephalus microplus*. PLoS Negl Trop Dis 2016;10:e0004298.

Bartíková P, Kazimírová M, Štibrániová I. Ticks and the effects of their saliva on growth factors involved in skin wound healing. J Venom Res 2020;10:45–52.

Bourke CD, Prendergast CT, Sanin DE, Oulton TE, Hall RJ, Mountford AP. Epidermal keratinocytes initiate wound healing and pro-inflammatory immune responses following percutaneous schistosome infection. Int J Parasitol 2015;45:215–24.

Chen YW, Yin S, Lai YJ, Johnson MD, Lin CY. Plasminogen-dependent matriptase activation accelerates plasmin generation by differentiating primary human keratinocytes. J Invest Dermatol 2016;136:1210–8.

Chmelar J, Calvo E, Pedra JH, Francischetti IM, Kotsyfakis M. Tick salivary secretion as a source of antihemostatics. J Proteomics 2012;75:3842–54.

Claesson-Welsh L, Dejana E, McDonald DM. Permeability of the endothelial barrier: identifying and reconciling controversies. Trends Mol Med 2021;27:314–31.

Corral-Rodríguez MA, Macedo-Ribeiro S, Barbosa Pereira PJ, Fuentes-Prior P. Tick-derived Kunitz-type inhibitors as antihemostatic factors. Insect Biochem Mol Biol 2009;39:579–95.

Deryugina EI, Quigley JP. Cell surface remodeling by plasmin: a new function for an old enzyme. J Biomed Biotechnol 2012;2012:564259.

Dixon WJ. Processing data for outliers. Biometrics 1953;9:74–89.

Fenton JW 2nd, Villanueva GB, Ofosu FA, Maraganore JM. Thrombin inhibition by hirudin: how hirudin inhibits thrombin. Haemostasis 1991;21:27–31.

Francischetti IM, Sa-Nunes A, Mans BJ, Santos IM, Ribeiro JM. The role of saliva in tick feeding. Front Biosci (Landmark Ed) 2009;14:2051–88.

Franta Z, Frantová H, Konvičková J, Horn M, Sojka D, Mareš M, et al. Dynamics of digestive proteolytic system during blood feeding of the hard tick *Ixodes ricinus*. Parasit Vectors 2010;3:119.

Grzegorski SJ, Hu Z, Liu Y, Yu X, Ferguson AC, Madarati H, et al. Disruption of the kringle 1 domain of prothrombin leads to late onset mortality in zebrafish. Sci Rep 2020;10:4049.

Jaiswal RK, Varshney AK, Yadava PK. Diversity and functional evolution of the plasminogen activator system. Biomed Pharmacother 2018;98:886–98.

Jennemann R, Sandhoff R, Langbein L, Kaden S, Rothermel U, Gallala H, et al. Integrity and barrier function of the epidermis critically depend on glucosylceramide synthesis. J Biol Chem 2007;282:3083–94.

Konnai S, Nishikado H, Yamada S, Imamura S, Ito T, Onuma M, et al. Molecular identification and expression analysis of lipocalins from blood feeding taiga tick, *Ixodes persulcatus* Schulze. exp Parasitol 2011;127:467–74. Exp Parasitol 2011.

Konnai S, Saito Y, Nishikado H, Yamada S, Imamura S, Mori A, et al. Establishment of a laboratory colony of taiga tick *Ixodes persulcatus* for tick-borne pathogen transmission studies. Jpn J Vet Res 2008;55:85–92.

Krishnaswamy S. Exosite-driven substrate specificity and function in coagulation. J Thromb Haemost 2005;3:54–67.

Lai R, Takeuchi H, Jonczy J, Rees HH, Turner PC. A thrombin inhibitor from the ixodid tick, *Amblyomma hebraeum*. Gene 2004;342:243–9.

Lane DA, Philippou H, Huntington JA. Directing thrombin. Blood 2005;106:2605–12.

Li WY, Chong SS, Huang EY, Tuan TL. Plasminogen activator/plasmin system: a major player in wound healing? Wound Repair Regen 2003;11:239–47.

Liao M, Zhou J, Gong H, Boldbaatar D, Shirafuji R, Battur B, et al. Hemalin, a thrombin inhibitor isolated from a midgut cDNA library from the hard tick *Haemaphysalis longicornis*. J Insect Physiol 2009;55:164–73.

Lund LR, Green KA, Stoop AA, Ploug M, Almholt K, Lilla J, et al. Plasminogen activation independent of uPA and tPA maintains wound healing in gene-deficient mice. EMBO J 2006;25:2686–97.

Macedo-Ribeiro S, Almeida C, Calisto BM, Friedrich T, Mentele R, Stürzebecher J, et al. Isolation, cloning and structural characterisation of boophilin, a multifunctional Kunitz-type proteinase inhibitor from the cattle tick. PLoS One 2008;3:e1624.

Morrison JF. Kinetics of the reversible inhibition of enzyme-catalysed reactions by tight-binding inhibitors. Biochim Biophys Acta 1969;185:269–86.

Nuttall PA. Tick saliva and its role in pathogen transmission. Wien Klin Wochenschr 2023;135:165–76.

Parizi LF, Ali A, Tirloni L, Oldiges DP, Sabadin GA, Coutinho ML, et al. Peptidase inhibitors in tick physiology. Med Vet Entomol 2018;32:129–44.

Pham M, Underwood J, Oliva Chávez AS. Changing the recipe: pathogen directed changes in tick saliva components. Int J Environ Res Public Health 2021;18:1806.

Qu Z, Chaikof EL. Interface between hemostasis and adaptive immunity. Curr Opin Immunol 2010;22:634–42.

Randolph SE. Tick-borne encephalitis incidence in Central and Eastern Europe: consequences of political transition. Microbes Infect 2008;10:209–16.

Rochlin I, Toledo A. Emerging tick-borne pathogens of public health importance: a mini-review. J Med Microbiol 2020;69:781–91.

Saraiva DG, Soares HS, Soares JF, Labruna MB. Feeding period required by *Amblyomma aureolatum* ticks for transmission of *Rickettsia rickettsii* to vertebrate hosts. Emerg Infect Dis 2014;20:1504–10.

Seeger MA, Paller AS. The roles of growth factors in keratinocyte migration. Adv Wound Care (New Rochelle) 2015;4:213–24.

Soares TS, Watanabe RM, Tanaka-Azevedo AM, Torquato RJ, Lu S, Figueiredo AC, et al. Expression and functional characterization of boophilin, a thrombin inhibitor from *Rhipicephalus* (*Boophilus*) *microplus* midgut. Vet Parasitol 2012;187:521–8.

Szabo I, Simon M Jr, Hunyadi J. Plasmin promotes keratinocyte migration and phagocytic-killing accompanied by suppression of cell proliferation which may facilitate re-epithelialization of wound beds. Clin Dev Immunol 2004;11:233–40.

Tirloni L, Braz G, Nunes RD, Gandara ACP, Vieira LR, Assumpcao TC, et al. A physiologic overview of the organ-specific transcriptome of the cattle tick *Rhipicephalus microplus*. Sci Rep 2020;10:18296.

Tirloni L, Kim TK, Coutinho ML, Ali A, Seixas A, Termignoni C, et al. The putative role of *Rhipicephalus microplus* salivary serpins in the tick-host relationship. Insect Biochem Mol Biol 2016;71:12–28.

Tirloni L, Reck J, Terra RM, Martins JR, Mulenga A, Sherman NE, et al. Proteomic analysis of cattle tick *Rhipicephalus* (*Boophilus*) *microplus* saliva: a comparison between partially and fully engorged females. PLoS One 2014;9:e94831.

Trapaidze A, Hérault JP, Herbert JM, Bancaud A, Gué AM. Investigation of the selectivity of thrombin-binding aptamers for thrombin titration in murine plasma. Biosens Bioelectron 2016;78:58–66.

Wikel S. Ticks and tick-borne pathogens at the cutaneous interface: host defenses, tick countermeasures, and a suitable environment for pathogen establishment. Front Microbiol 2013;4:337.

Wu XB, Na RH, Wei SS, Zhu JS, Peng HJ. Distribution of tick-borne diseases in China. Parasit Vectors 2013;6:119.

Yang X, Chen X. The crosstalk between the blood-brain barrier dysfunction and neuroinflammation after general anaesthesia. Curr Issues Mol Biol 2022;44:5700–17.

Zohrabian VM, Forzani B, Chau Z, Murali R, Jhanwar-Uniyal M. Rho/ROCK and MAPK signaling pathways are involved in glioblastoma cell migration and proliferation. Anticancer Res 2009;29:119–23.

SUPPLEMENTARY MATERIALS AND METHODS

Reagents

MCDB 131 (microvascular endothelial cell medium), epidermal GF, hydrocortisone, glutamine, fetal calf serum, penicillin/streptomycin, trypsin-EDTA (0.25%), and trypsin neutralizer solution were purchased from Life Technologies (Carlsbad, CA). CnT-07 epithelial proliferation medium was obtained from CellnTec Advanced Cell Systems (Bern, Switzerland). Purified human α-thrombin, γ-thrombin, factor XIa, factor XIIa-α, factor XIIa-β, kallikrein, activated protein C, plasmin, factor Xa, and fibrinogen were sourced from Enzyme Research Laboratories (South Bend, IN). Human neutrophil elastase, porcine pancreatic elastase, human urokinase plasminogen (PLG) activator, human tissue-type PLG activator, and human cathepsin G were purchased from Molecular Innovations (Novi, MI). Human chymase, bovine α-chymotrypsin, porcine trypsin, bivalirudin, human antithrombin III, Glu-type human PLG, [Tyr(SO3H)]63]-Hirudin fragment 54-65, human plasma, *E coli* O111:B4 lipopolysaccharide, and FITC-Dextran 70,000 were procured from Sigma-Aldrich/EMD Millipore (Saint Louis, MO). A complete list of all chromogenic substrates and their suppliers is provided in Supplementary Table S1. All other chemicals were of analytical grade and were commercially available.

Ticks

Adult *Ixodes persulcatus* ticks were obtained from a laboratory colony fed on pathogen-free Syrian hamsters maintained in a P3 animal facility at the Graduate School of Veterinary Medicine, Hokkaido University (Sapporo, Japan) (Konnai et al, 2008). The protocols of all animal experiments were approved by the Ethics Committee of the Faculty of Veterinary Medicine, Hokkaido University (22-0035).

Mice

Adult male C57BL/6J mice aged 4–6 weeks and weighing 15–20 g were obtained from Charles River Laboratories. Throughout the experiment, the mice were housed in the animal facility at our institution, the Rocky Mountain Veterinary Branch, located at Rocky Mountain Laboratories (Hamilton, MT). The mice were kept under controlled conditions, with temperatures maintained between 20 and 24 °C and a relative air humidity of 40–60%. They were subjected to a 12-hour dark/light cycle and provided free access to water and food. All procedures involving the mice were conducted in accordance with the National Institutes of Health Guide for the Care and Use of Laboratory Animals. Our experimental protocol received approval from the Animal Care and Use Committee at Rocky Mountain Laboratories (number 2020-045).

Tick dissection, RNA extraction, and cDNA library construction

For RNA extraction, both partially and fully engorged adult females of *I persulcatus* ticks were washed with 70% ethanol and dissected in a Petri dish containing cold 20 mM PBS at pH 7.2. Dissection was performed using a scalpel blade under a light microscope. To analyze the expression profile, we collected unfed and fed larvae (denoted as ULA and FLA, respectively), unfed and fed nymphs (denoted as UNY and FNY, respectively), unfed adult females (denoted as UAF), 1-day–fed female salivary glands (denoted as 1SG), 4-day–fed female salivary glands (denoted as 4SG), gut (denoted as 4G), and carcass (denoted as CA; whole tick without SG, G, and OV), fully fed female salivary glands (denoted as FSG), ovary (denoted as FOV), and unfed adult males (denoted as UAM). These samples were macerated in TRIzol reagent (Invitrogen) for RNA extraction. RNA isolation followed the manufacturer's instructions, and total RNA was treated with DNase I (Invitrogen) to remove any contaminating DNA. RNA yield and quality were assessed using a spectrophotometer (Amersham Biosciences, Pharmacia Biotech, Ultraspec 1000). To construct the *I persulcatus* cDNA library, total RNA extracted from whole adult female ticks was used. For cDNA synthesis, the Superscript III kit (Invitrogen) was employed following the manufacturer's instructions. Subsequently, the cDNA library was generated using the SMART cDNA Library Construction Kit (Clontech, Takara Bio Company) as per the manufacturer's instructions.

Persulcatin sequence amplification and cloning

Sequences encoding Kunitz-type inhibitors from other tick species, which were deposited in the GenBank database, were employed as queries and searched against the *I scapularis* database using the BLAST (Basic Local Alignment and Search Tool) algorithm (Altschul et al, 1997). To amplify the full-length open reading frame sequence from *I persulcatus* corresponding to persulcatin, primers based on the *I scapularis* sequence XM_002403992, available in the National Center for Biotechnology Information database, were designed. The PCR reaction was carried out using the Elongase enzyme (Invitrogen) under the following conditions: initial denaturation at 95 °C for 5 minutes, followed by 35 cycles of denaturation at 94 °C for 30 seconds, annealing at 58 °C for 30 seconds, and extension at 68 °C for 2 minutes. A final extension step was performed at 68 °C for 5 minutes. The resulting amplification products were separated using 0.8% agarose gel electrophoresis and then purified using the Geneclean kit (BIO 101, Q-BIOgene), following the manufacturer's instructions. The obtained amplicon was cloned into the pGEM-T plasmid (Promega) and introduced into *E coli* DH5α host strain using the manufacturer's instructions. Verification of successful cloning was accomplished through DNA sequencing.

Bioinformatic analysis

The deduced amino acid sequence was analyzed using Compute pI/Mw in ExPASy molecular biology server (Gasteiger et al, 2003). The putative domain architecture and functional sites were identified using ScanProsite (Sigrist et al, 2012) and InterProScan (Hunter et al, 2009). Sequences were aligned using the MUSCLE algorithm (Edgar, 2004). The secretory signal peptide and cleavage site for the mature protein were predicted by SignalP server, version 4.1 (Nielsen, 2017) . The phylogenetic analysis was performed by the neighbor-joining method using the MEGA 11 software (Tamura et al, 2021) with 1000 replicates bootstrap support. The AlphaFold2 program (Jumper et al, 2021) was used to predict the tertiary structures of persulcatin. The program was run locally on the National Institutes of Health Biowulf cluster in a Linux environment using the monomer mode.

Structures were visualized, and figures were generated using PyMol (The PyMOL Molecular Graphics System, version 2.6.0a0, Schrödinger, LLC).

Transcriptional profiling analysis of persulcatin gene

The transcriptional profile of the persulcatin gene was evaluated in *I persulcatus* male and female different tissues and developmental stages by RT-PCR using specific primers. Tick actin was used as internal RT-PCR control (Sajiki et al, 2022). Reaction products were analyzed by agarose electrophoresis.

Recombinant expression and protein purification

The mature protein-coding sequence (without the predicted signal peptide) was codon optimized for mammalian expression, synthesized, and cloned into VR2001 vector in frame with tissue-type PLG activator signal peptide sequence containing a 6x-histidine tag followed by an enterokinase cleavage site (BioBasic, Markham, Canada). Plasmid DNA was purified using NucleoBond PC 2000 plasmid kit (Takara, Shiga, Japan). Expi293 human embryonic kidney cells (Thermo Fisher Scientific, Waltham, MA) were transfected with endotoxin-free plasmid. Supernatants were collected 72 hours after transfection, centrifuged (1000*g* per 15 minutes) and frozen. Recombinant protein was purified by affinity, ion exchange, and size-exclusion chromatography. The supernatant containing the secreted recombinant protein was incubated for 1 hour at room temperature with AmMag Ni Magnetic beads (GenScript, Piscataway, NJ) previously pre-equilibrated with PBS, pH 7.4 supplemented with Tween-20 0.05%. Then, beads were washed with the binding buffer, followed by PBS, pH 7.4, and an extra wash with PBS, pH 7.4 supplemented with 5 mM imidazole. The recombinant protein was eluted using PBS, pH 7.4 supplemented with 500 mM imidazole. The protein fractions were visualized in a 4–20% SDS-PAGE followed by Coomassie blue staining. The fractions of interest were pooled, concentrated, and dialyzed against 20 mM Tris-hydrogen chloride (HCl), pH 8.0 using an Amicon Ultra-15 centrifugal filter units (MilliporeSigma) and used for the subsequent ion exchange chromatography. The sample was applied on a pre-equilibrated HiTrap Q column followed by a washing step with 5-column volumes of 20 mM Tris-HCl, pH 8.0 buffer. The recombinant protein was eluted by passing a linear gradient of 20 mM Tris-HCl, 1 M sodium chloride (NaCl), pH 8.0 buffer using an AKTA start chromatography system (Cytiva). Eluted fractions were visualized in a 4–20% SDS-PAGE followed by Coomassie blue staining. The fractions of interest were pooled, concentrated, and dialyzed against 20 mM Tris-HCl, 150 mM NaCl, pH 7.4 buffer using Amicon Ultra-15 centrifugal filter units (MilliporeSigma) and used for the subsequent gel filtration chromatography. The sample was loaded on a Superdex 75 10/300 GL column, and proteins were eluted isocratically at a flow rate of 0.5 ml/minute in 20 mM Tris-HCl, 150 mM NaCl, pH 7.4 buffer. The protein fractions were visualized in a 4–20% SDS-PAGE followed by Coomassie blue staining, the fractions of interest were pooled, and protein concentration was determined by BCA (Thermo Fisher Scientific, Waltham, MA). Purified protein was stored at −80 °C upon use.

Serine protease inhibition screening

The inhibitory potential of persulcatin was tested against the following proteases: human α-thrombin (2 nM), human γ-thrombin (5 nM), human factor XIa (5 nM), human factor XIIa-α (10 nM), human factor XIIa -β (10 nM), plasma kallikrein (1 nM), human activated protein C (5 nM), human plasmin (10 nM), human factor Xa (5 nM), human chymase (10 nM), bovine pancreatic α-chymotrypsin (10 nM), porcine pancreatic trypsin (5 nM), human neutrophil elastase (20 nM), porcine pancreatic elastase (50 nM), human urokinase PLG activator (10 nM), human tissue-type PLG activator (20 nM), and human cathepsin G (50 nM). Briefly, persulcatin (1 μM) was preincubated with each protease for 15 minutes in 20 mM Tris-HCl, 150 mM NaCl, 0.01% Tween-20, pH 7.4 at 37 °C. After incubation, different synthetic chromogenic substrates (200 μM) designed specifically for each protease were added in a final volume of 100 μl using a 96-well plate. A complete list with all substrates used can be found in Supplementary Table S1. The substrate hydrolysis rate at 30 °C was followed at 405 nm in kinetic mode in a Synergy H1 max micro plate reader (Biotek, Santa Clara, CA) for 15 minutes. The observed substrate hydrolysis rate in the absence of persulcatin was considered 100% and compared with the remaining enzymatic activity in the presence of persulcatin. Data are presented as mean ± standard error of triplicate readings.

Mechanisms of plasmin inhibition

Plasmin inhibition by persulcatin was characterized using classical methods of enzyme kinetic analysis. The enzyme (10 nM) was preincubated at 37 °C for 15 minutes with different concentrations of persulcatin (0, 0.01, 0.05, 0.1, 0.5, 1, and 2 μM) in a reaction media containing 20 mM Tris-HCl, 150 mM NaCl, 0.01% Tween-20, pH 7.4. The remaining plasmin activity was measured by the addition of S-2251 substrate (200 μM) in a volume of 100 μl. The amount of *p*-nitroaniline produced was monitored at 405 nm in intervals of 14 seconds for 30 minutes using a Synergy H1 max micro plate reader (Biotek). The progress curves were obtained by plotting absorbance values (A405 nm) versus time (s). For all calculations, the initial rate of hydrolysis was chosen to determine the steady-state kinetics (Vmax mode) of persulcatin–plasmin interaction. Slow- or fast-binding mode was determined by analyzing the progress curves with or without 45-minute preincubation time between enzyme plus inhibitor. To determine the type of inhibition, binding mode, and kinetic constants (half-maximal inhibitory concentration, apparent K_i, and real K_i), a dose–response plot of fractional velocity (V_i/V_o) as a function of persulcatin (0–1 μM) was constructed in the presence of different plasmin (6.5, 12.5, and 25 nM) or S-2251 (0.1, 0.2, 0.4, and 0.5 mM) concentrations. In these cases, V_i was the inhibited steady-state velocity, and V_o was the control (uninhibited) velocity. A positive linear regression obtained by plotting half-maximal inhibitory concentration values as a function of enzyme concentration was used to determine the tight-binding mode of inhibition, whereas the y-intercept indicated the apparent K_i (K_i^{app}). The tight-binding behavior was also confirmed by fitting the fractional velocity in the presence of different substrate concentrations to the Morrison equation. The type

of inhibition (competitive, noncompetitive, or uncompetitive) was determined by the slope of half-maximal inhibitory concentration plotted as a function of S-2251 concentration, and the real K_i value was estimated by the Dixon's plot ($1/V_i$ vs inhibitor concentration) (Dixon, 1953). All data points from kinetic measurements were fitted using GraphPad Prism software (GraphPad Software, San Diego, CA). Data are the mean of 3 determinations, each performed in triplicates.

Mechanisms of thrombin inhibition

Human α-thrombin (2.5 nM) was preincubated at 37 °C for 15 minutes with different concentrations of persulcatin (0, 0.01, 0.05, 0.1, 0.5, 1, and 2 μM) in a reaction media containing 20 mM Tris-HCl, 150 mM NaCl, 0.01 % Tween-20, pH 7.4. The remaining thrombin activity was measured by the addition of human fibrinogen as substrate (2 mg/ml) in a volume of 150 μl. Fibrinocoagulation process was then followed by the increase in optical density at 650 nm in intervals of 14 seconds for 30 minutes using a Synergy H1 max micro plate reader (Biotek). The type of inhibition, binding mode, and kinetic constants were all determined following the same method described earlier for plasmin. α-Thrombin inhibition was also compared in the presence of specific α-thrombin exosite-1 (hirudin) or active-site (bivalirudin and antithrombin III) inhibitors. Briefly, 2.5 nM α-thrombin was incubated in the presence of different concentrations (0, 0.01, 0.05, 0.1, 0.5, 1.0, and 2.0 μM) of persulcatin, hirudin, bivalirudin, or antithrombin III. The remaining enzyme activity was then measured by the addition of macromolecular substrate fibrinogen or the peptide-based chromogenic substrate S-2238 following the procedure described earlier. The displacement of bivalirudin or antithrombin III from its binding site was also evaluated in the presence of persulcatin. In these cases, bivalirudin (0−2 μM) or antithrombin III (0−0.4 μM) was preincubated (30 minutes) with α-thrombin (2.5 nM), followed by the addition of increasing concentrations of persulcatin (0, 0.5, 1.0, and 2.0 μM) and the substrate S-2238 (200 μM). Similarly, in some experiments, γ-thrombin activity (a thrombin variant that has its exosite-1 deleted) was also measured in the presence of bivalirudin (1 μM), persulcatin (1 μM), hirudin (1 μM), or antithrombin III (0.2 μM) using S-2238 as substrate. For all the experiments, data represent the mean of 3 determinations, each performed in triplicates.

Blood coagulation in vitro

The recalcification profile of normal citrated human plasma was evaluated by kinetic assay using a Synergy H1 max micro plate reader (Biotek). Briefly, plasma (50 μl) was incubated at 37 °C with 2 μM persulcatin in Tris-buffered saline, pH 7.4 (150 μl, final volume). Then, coagulation was triggered by 10 mM calcium chloride, and the increase in optical density was monitored at 650 nm for 30 minutes. Activated partial thromboplastin time and prothrombin time were evaluated on a STart 4 coagulometer (Diagnostica Stago, Parsippany-Troy Hills, NJ). For the activated partial thromboplastin time assay, plasma (50 μl) was incubated with different concentrations of persulcatin (1−3 μM volume of 10 μl) or the same Tris-buffered saline volume (control) and placed in the coagulometer for 10 minutes at 37 °C. After, 50 μl of prewarmed activated partial thromboplastin time reagent (STA PTT; Diagnostica Stago) was added and incubated for 3 minutes at 37 °C. Calcium chloride (50 μl at 25 mM) was added to start reactions. Time for clot formation was recorded in quadruplicate in 2 independent replicates. For the prothrombin time, plasma (50 μl) was incubated with different concentrations of persulcatin (1−3 μM volume of 10 μl) or the same Tris-buffered saline volume (control) and placed in the coagulometer for 10 minutes at 37 °C. Then, 100 μl of the prothrombin time reagent (NEOplastine CI plus; Diagnostica Stago) was added. Time for clot formation was recorded in quadruplicate in 2 independent replicates.

Endothelial cell−based coagulation assay

Human dermal microvascular endothelial cells (human microvascular endothelial cell 1, ATCC CRL-3243) were cultured in MCDB 131 supplemented with epidermal GF (10 ng/ml), hydrocortisone (1 μg/ml), glutamine (10 mM), and fetal bovine serum (10%). The cells were maintained without antibiotics in a 37 °C/5% carbon dioxide environment following the standard procedures for cell culture. Cells (1×10^3) were cultured in 96-well plates until they reached a confluent monolayer. A procoagulant profile was induced by activating the endothelial cells for 2, 6, and 24 hours with 1 μg/ml lipopolysaccharide (O111:B4) in the absence of fetal bovine serum. After lipopolysaccharide treatments, culture media was removed, and human plasma (50 μl) was added in the presence or absence of different concentrations of persulcatin (0−2 μM) in a final volume of 150 μl. The coagulation process was triggered by 10 mM calcium chloride, and the clot formation was followed directly on endothelial cell monolayers at 650 nm for 40 minutes using a Cytation 5 multimode reader (Biotek). The coagulation time (measured in seconds [s] was defined as the time taken to reach the 0.05 absorbance value [onset optical density]). All data points represent the mean of 3 determinations, each performed in triplicates.

Endothelial cell permeability assay

Endothelial cell permeability was studied by the FITC-dextran method using transwell inserts (12 mm × 0.4 μm) (Millicell Cell Culture Insert, Merck). Human microvascular endothelial cell 1 (5×10^4 cells per transwell insert) were plated on 1% gelatin-coated inserts (24 wells) and cultured for 7 days to form a 100% confluent monolayer inside each insert. Then, the inserts were divided and treated according to the following groups (n = 4 per group per plate): (i) PBS, (ii) α-thrombin (50 nM), (iii) α-thrombin (50 nM) + persulcatin (1 μM), and (iv) persulcatin (1 μM). The upper chamber received the treatments in Krebs-Ringer bicarbonate buffer containing 2 g/l BSA and FITC-dextran (70 kDa, 1 mg/ml) in a total volume of 200 μl. The lower chamber received only Krebs-Ringer buffer in a total volume of 500 μl. FITC-dextran leakage to the lower chamber was measured in duplicates for each insert at 15, 30, 60, 120, and 240 minutes using the Cytation 5 multimode reader (Biotek) (485 nm excitation/528 nm emission). During the experiment, cells were kept in a 37 °C/5% carbon dioxide environment. The alteration of membrane permeability was also detected by crystal violet stain. In brief, inserts containing cells were fixed with 4% paraformaldehyde for 15 minutes, stained with 1% crystal violet for 30 minutes, and finally washed 3 times with PBS. Images

were captured with the Cytation 5 multimode reader (Biotek). Alternatively, endothelial cell permeability was evaluated by vascular endothelial-cadherin immunocytochemistry. In this case, 100% confluent human microvascular endothelial cells 1 were treated with PBS, thrombin (50 nM), thrombin (50 nM) plus persulcatin (1 μM), and persulcatin (1 μM). After 4 hours at 37 °C/5% carbon dioxide environment, cells were fixed in methanol, permeabilized in Tris-buffered saline/0.1% Tween, blocked in normal goat serum (10%), and processed for overnight immunolabeling with vascular endothelial-cadherin antibody (working dilution 5 μg/ml) (Life Technologies, Carlsbad, CA). The secondary antibody was a 448-fluorescence conjugated goat anti-rabbit IgG at a dilution of 1:1000 (Life Technologies), and nuclei were counterstained with Hoechst. Fluorescently labeled images were captured using the Cytation 5 multimode reader (Biotek).

Ex vivo aortic ring assay

Adult male C57BL/6J mice weighing 15–20 g (n = 8) were killed by isoflurane overdose followed by cervical dislocation. Abdominal aorta was dissected from surrounding tissues, and the aortic rings (approximately 2 mm) were prepared, washed, and resuspended in Krebs-Ringer buffer. Three rings per mouse were individually placed in each well of a 96-well plate, incubated at 37 °C for 5 minutes in Krebs-Ringer buffer, and divided into 4 treatment groups: (i) PBS, (ii) α-thrombin (50 nM), (iii) α-thrombin (50 nM) plus persulcatin (1 μM), and (iv) persulcatin (1 μM). The rings were incubated for 4 hours in a 37 °C/5% carbon dioxide environment and then processed for tissue factor protein expression analysis by western blot. The following antibody was used: anti–tissue factor antibody (H-9) (working dilution 1:200) (number SC-374441, Santa Cruz Biotechnology, Dallas, TX).

PLG–plasmin system activation on keratinocyte surface

Mouse epidermal keratinocytes (COCA cell line, ECACC 10112001) were maintained in CnT-07 epithelial proliferation medium (CellnTec, Bern, Switzerland), following the manufacturer's instructions. PLG activation was estimated directly on the surface of confluent COCA cells cultured on 24-well plates in a complete medium. In the first set of experiments, different concentrations of human PLG (0, 100, 200, and 400 nM) were added to the cells, and plasmin generation was monitored at 0, 15, 30, 60, 120, and 240 minutes. Plasmin-like activity at the different time points was estimated in conditioned medium through S-2251 hydrolysis, following the procedure described earlier for enzyme activity measurements. A similar experiment was also designed, but in this case, keratinocytes were treated with PBS, 200 nM PLG, 200 nM PLG plus 1 μM persulcatin, and 1 μM persulcatin before plasmin determinations. Plasmin formation was also demonstrated by fibrin degradation assays. For this purpose, conditioned media obtained from keratinocytes treated with PLG and/or persulcatin were submitted to a zymogram using fibrin as substrate, in which a polyacrylamide gel was copolymerized with a mixture containing 12 mg/ml human fibrinogen plus 50 nM thrombin. After SDS removal with 2.5% Triton X-100 solution, formed plasmin was detected as a single clear band of fibrinolysis against a blue background of undigested fibrin substrate. Alternatively, fibrin degradation was also followed in a kinetic assay. In this case, a fibrin clot was produced by incubating (30 minutes/37 °C) fibrinogen (2 mg/ml) + thrombin (50 nM) in a final volume of 150 μl in a 96-well plate. Then, conditioned media (20 μl) from keratinocytes were carefully added to the top of each fibrin clot. Human-purified plasmin (12.5 nM) was used as a positive control for fibrin degradation. The fibrin degradation process was monitored by optical density decrease at 650 nm.

PLG–plasmin–induced keratinocyte migration

Keratinocyte (COCA cell line) migration was evaluated by the scratch-induced wound healing assay directly on cell monolayers. One hundred percent confluent COCA cells cultured on 24-well plates were used and kept in complete CnT-07 medium during the entire experiment. A minimum of 4 plates were run for each experiment. A scratch wound was induced on cell monolayers using the BioTek AutoScratch equipment (Biotek), allowing to creation of automatically reproducible scratch wounds per well. Next, the wounded cells were treated with increasing concentrations of human PLG (100, 200, and 400 nM) or PBS. Optical bright field images were captured at the beginning (0 hours) and every 2 hours for a total time of 24 hours in a Cytation 5 multimode reader. The wound confluence was estimated by the area of cells recovering the gap induced by the scratch. Gap areas were measured and compared by the AutoScratch app (Biotek). In another set of experiments, scratch-induced wound healing assay was also performed in the presence of PBS, 200 nM PLG, 200 nM PLG plus 1 μM persulcatin, and 1 μM persulcatin. Plasmin-like activity generated after the scratch-induced wound healing experiments (total time of 24 hours) was estimated in keratinocyte-conditioned media through S-2251 hydrolysis following the procedure described earlier for enzyme activity measurements.

Matrix protein analysis

Conditioned media from keratinocytes treated with PLG and/or persulcatin as obtained in item 10.1.18 were used to analyze the protein content of matrix metalloproteinases 2 and matrix metalloproteinase 9, fibronectin, and collagen-1A1 by western blot. The following antibodies were used: mouse/rat matrix metalloproteinase 2 (working dilution 1:500) (number AF1488, R&D Systems, Minneapolis, MN), mouse/rat matrix metalloproteinase 9 (working dilution 1:500) (number AF909, R&D Systems), fibronectin (working dilution 1:200) (number 610077, BD Biosciences, Franklin Lakes, NJ), and collagen-1A1 (working dilution 1:200) (number C-59772, Santa Cruz Biotechnology).

Western blot

For western blot analysis, protein samples were reduced with 10% β-mercaptoethanol, separated using Mini-PROTEAN TGX stain-free precast gels (Bio-Rad Laboratories, Hercules, CA) and transferred in a Trans-Blot Turbo transfer system (Bio-Rad Laboratories). Blots were probed using the respective antibodies described earlier and processed by chemiluminescence detection following the classical standard procedures. Images were acquired in a ChemiDoc MP Imaging System (Bio-Rad Laboratories).

SUPPLEMENTARY REFERENCES

Altschul SF, Madden TL, Schäffer AA, Zhang J, Zhang Z, Miller W, et al. Gapped BLAST and PSI-BLAST: a new generation of protein database search programs. Nucleic Acids Res 1997;25:3389–402.

Dixon WJ. Processing data for outliers. Biometrics 1953;9:74–89.

Edgar RC. MUSCLE: multiple sequence alignment with high accuracy and high throughput. Nucleic Acids Res 2004;32:1792–7.

Gasteiger E, Gattiker A, Hoogland C, Ivanyi I, Appel RD, Bairoch A. Expasy: the proteomics server for in-depth protein knowledge and analysis. Nucleic Acids Res 2003;31:3784–8.

Hunter S, Apweiler R, Attwood TK, Bairoch A, Bateman A, Binns D, et al. InterPro: the integrative protein signature database. Nucleic Acids Res 2009;37:D211–5.

Jumper J, Evans R, Pritzel A, Green T, Figurnov M, Ronneberger O, et al. Highly accurate protein structure prediction with AlphaFold. Nature 2021;596:583–9.

Konnai S, Saito Y, Nishikado H, Yamada S, Imamura S, Mori A, et al. Establishment of a laboratory colony of taiga tick *Ixodes persulcatus* for tick-borne pathogen transmission studies. Jpn J Vet Res 2008;55:85–92.

Nielsen H. Predicting secretory proteins with SignalP. In: Kihara D, editor. Protein function prediction. New York: Humana Press; 2017. p. 59–73.

Sajiki Y, Konnai S, Okagawa T, Maekawa N, Isezaki M, Yamada S, et al. Suppressive effects of *Ixodes persulcatus* sialostatin L2 against Borrelia miyamotoi-stimulated immunity. Ticks Tick Borne Dis 2022;13:101963.

Sigrist CJA, De Castro E, Cerutti L, Cuche BA, Hulo N, Bridge A, et al. New and continuing developments at PROSITE. Nucleic Acids Res 2012;41(D1):D344–7.

Tamura K, Stecher G, Kumar S. MEGA11: molecular evolutionary genetics analysis version 11. Mol Biol Evol 2021;38:3022–7.

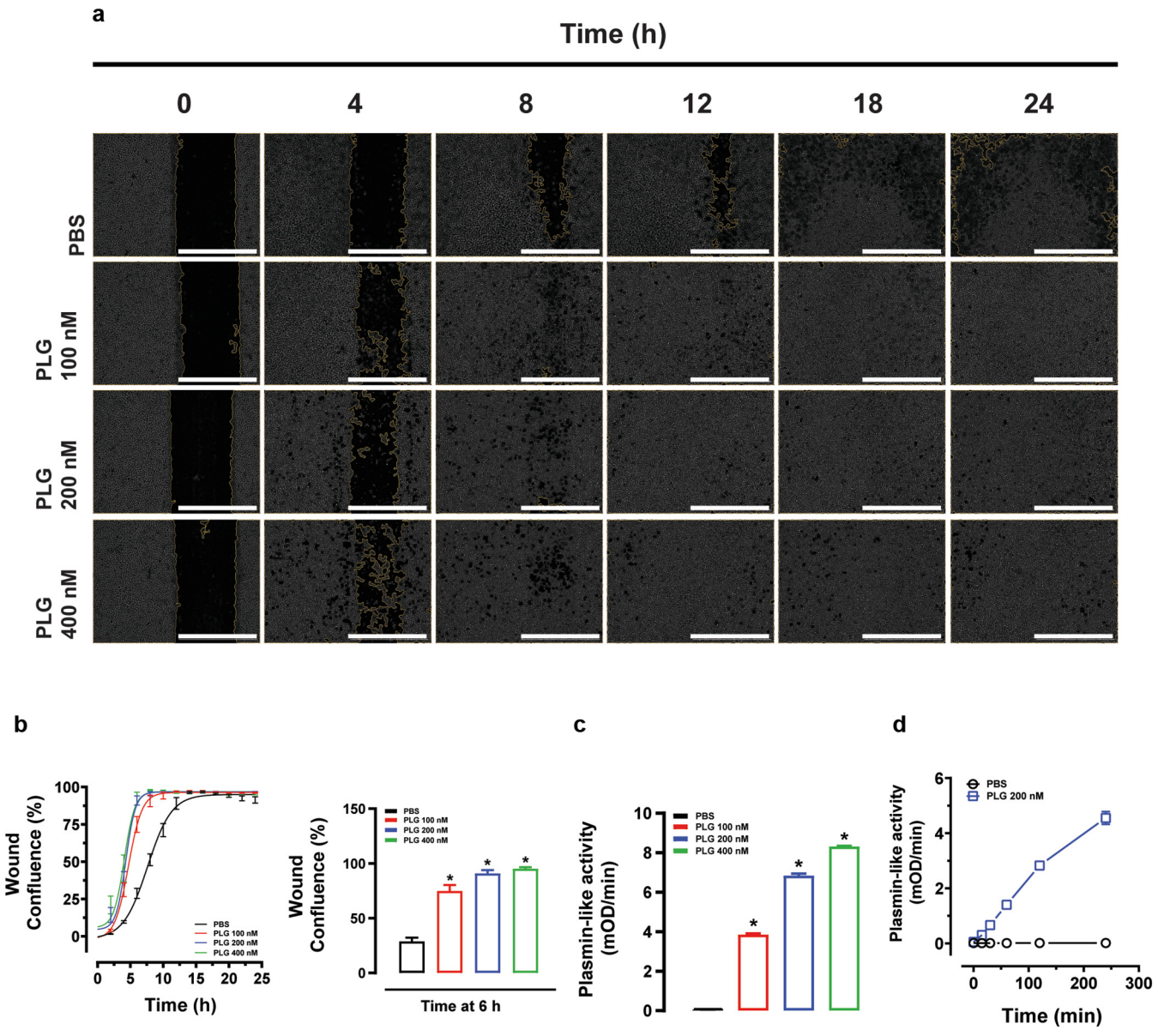

Supplementary Figure S1. PLG is activated on the surface of keratinocytes generating plasmin and inducing cell migration. (**a**) Keratinocyte (COCA cell line) migration was estimated in the presence of PBS and increasing concentrations of human PLG using the classical scratch-induced wound healing assay in cell monolayers. Representative images are shown indicating the wound closure over time until 24 h. (**b**) Quantitative analysis of keratinocyte migration after PLG administration. (**c**) Plasmin-like activity generated in the keratinocyte-conditioned media as estimated on the basis of S-2251 hydrolysis. (**d**) Time-point kinetics for plasmin generation on the surface of keratinocytes. Cells were treated with 200 nM PLG, and after different time points (0, 5, 15, 30, 60, 120, 240 min), the formed plasmin was estimated by S-2251 hydrolysis. h, hour; min, minute; PLG, plasminogen.

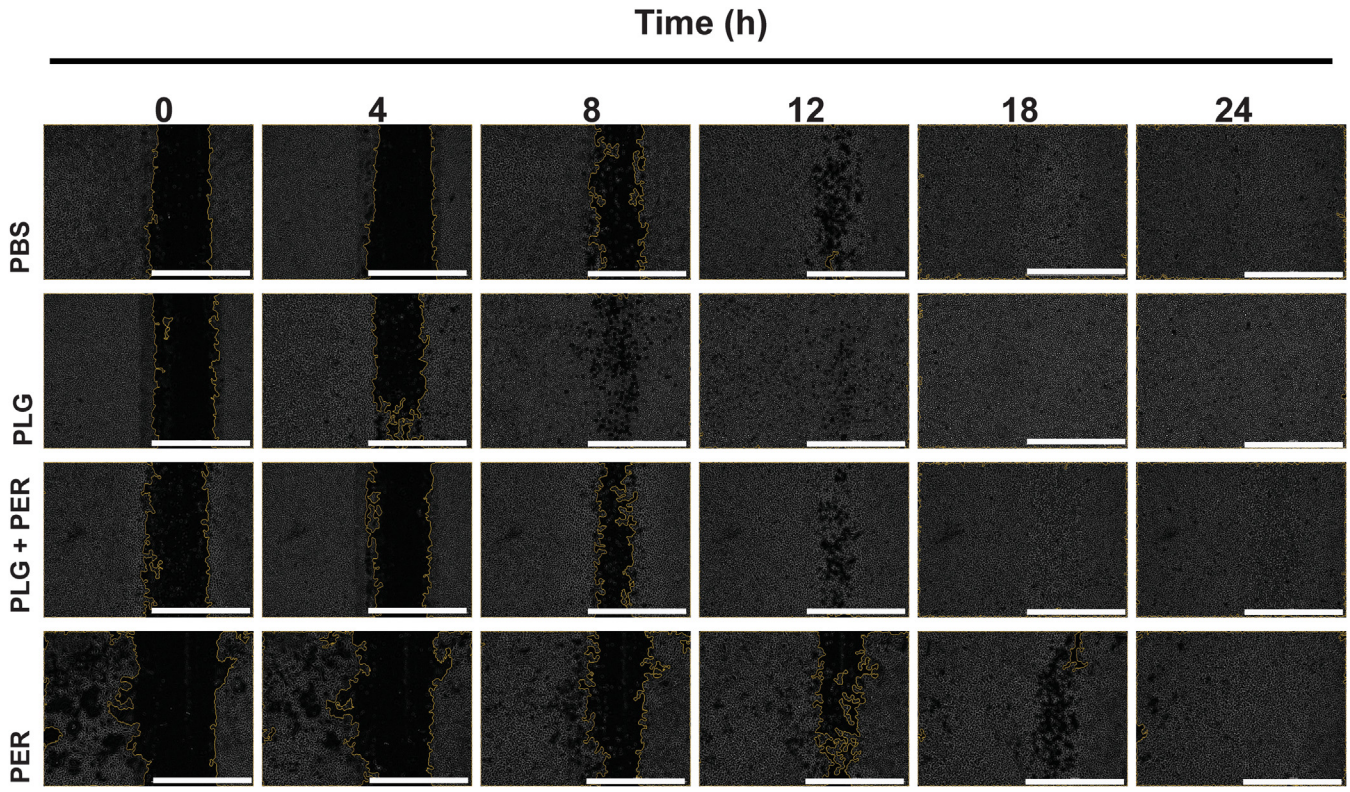

Supplementary Figure S2. Persulcatin inhibits the keratinocyte migration induced by plasmin. Representative images from the experiment are shown in Figure 3. Keratinocyte (COCA cell line) migration was estimated in the presence of PBS, 200 nM PLG, and/or 1 μM PER using the classical scratch-induced wound-healing assay in cell monolayers. The images are showing the wound closure over time until 24 h. h, hour; PER, persulcatin; PLG, plasminogen.

Supplementary Table S1. List of Chromogenic Substrates Used in This Work

Substrate[1]	Sequence	Protease Specificity	Company
Chromogenix S-2238	H-D-Phe-L-Pip-Arg-pNA	α-thrombin, γ-thrombin	Diapharma
Chromogenix S-2222	Bz-Ile- Glu(γ-OR)-Gly-Arg-pNA	Factor Xa	Diapharma
Chromogenix S-2302	H-D-Pro-Phe-Arg-pNA	Factor XIa, Factor XIIa-α, Factor XIIa-β and plasma kallikrein	Diapharma
Chromogenix S-2251	H-D-Val-Leu-Lys-pNA	Plasmin	Diapharma
Calbiochem 324696	MeOSuc-Ala-Ala-Pro-Val-pNA	Human neutrophil elastase	Calbiochem
Chromogenix S-2288	H-D-Ile-Pro-Arg-pNA	Tissue-type plasminogen activator and trypsin	Diapharma
Chromogenix S-7388	N-Succinyl-Ala-Ala-Pro-Phe-pNA	Cathepsin G, chymotrypsin, and chymase	Diapharma
Chromogenix S-2366	L-PyroGlu-Pro-Arg-pNA	Activated protein C	Diapharma
Chromogenix S-4760	N-Succinyl-Ala-Ala-Ala-pNA	pancreatic elastase	Diapharma
Chromogenix S-2444	pyroGlu-Gly-Arg-pNA	Urokinase-type plasminogen activator	Diapharma

[1]In general experiments, the final concentration used for each substrate was 200 μM. Different concentrations were used just to determine thrombin and plasmin mechanisms of inhibition, as detailed in the extended material and methods.